

UKAEA-CCFE-PR(21)83

D.J.M. King, A.J. Knowles, D. Bowden, M.R.  
Wenman, S. Capp, M. Gorley, J. Shimwell, L. Packer,  
M.R. Gilbert, A. Harte

# High Temperature Zirconium Alloys for Fusion Energy

Enquiries about copyright and reproduction should in the first instance be addressed to the UKAEA Publications Officer, Culham Science Centre, Building K1/O/83 Abingdon, Oxfordshire, OX14 3DB, UK. The United Kingdom Atomic Energy Authority is the copyright holder.

The contents of this document and all other UKAEA Preprints, Reports and Conference Papers are available to view online free at [scientific-publications.ukaea.uk/](https://scientific-publications.ukaea.uk/)

# High Temperature Zirconium Alloys for Fusion Energy

D.J.M. King, A.J. Knowles, D. Bowden, M.R. Wenman, S. Capp, M.  
Gorley, J. Shimwell, L. Packer, M.R. Gilbert, A. Harte



# High Temperature Zirconium Alloys for Fusion Energy

DJM King<sup>1,2</sup>, AJ Knowles<sup>2,3</sup>, D Bowden<sup>1</sup>, MR. Wenman<sup>2</sup>, S. Capp<sup>1</sup>, M Gorley<sup>1</sup>, J Shimwell<sup>1</sup>,  
L Packer<sup>1</sup>, MR Gilbert<sup>1</sup>, A Harte<sup>1</sup>

<sup>1</sup>United Kingdom Atomic Energy Authority (UKAEA), Culham Science Centre, Abingdon, OX14 3DB, United Kingdom

<sup>2</sup>Centre for Nuclear Engineering, Imperial College London, South Kensington, London, SW7 2AZ, United Kingdom

<sup>3</sup>School of Metallurgy & Materials, University of Birmingham, Birmingham, UK

**Abstract.** This Review considers current Zr alloys and opportunities for advanced zirconium alloys to meet the demands of a structural material in fusion reactors. Zr based materials in the breeder blanket offer the potential to increase the tritium breeding ratio above that of Fe, Si and V based materials. Current commercial Zr alloys might be considered as a material in water-cooled breeder blanket designs, due to the similar operating temperature to fission power plants. For breeder blankets designed to operate at higher temperatures, current commercial Zr alloys will not meet the high temperature strength and thermal creep requirements. Hence, Zr alloys with an operational temperature capability beyond that of current commercial fission alloys have been reviewed, specifically: binary Zr alloy systems Zr-Al, Zr-Be, Zr-Cr, Zr-Nb Zr-Ti, Zr-Si, Zr-Sn, Zr-V and Zr-W; as well as higher order Zr alloys Zr-Mo-Ti, Zr-Nb-Ti, Zr-Ti-Al-V and Zr-Mo-Sn. It is concluded that, with further work, higher order Zr alloys could achieve the required high temperature strength, alongside ductility, while maintaining a low thermal neutron cross-section. However, there is limited data and uncertainty regarding the structural performance and microstructural stability of the majority of advanced Zr alloys for temperatures 500-700°C, at which they would be expected to operate for helium- and liquid metal-cooled breeder blanket designs.

**Keywords:** Zirconium alloys, Tritium breeder, high temperature materials

## Contents

1.	Introduction.....	2
2.	Current Zr alloys .....	6
2.1.	Material properties .....	6
2.2.	Effect of impurities (C, H, Li, and N).....	10
2.2.1.	Carbon .....	10
2.2.2.	Hydrogen .....	10
2.2.3.	Helium .....	11
2.2.4.	Lithium .....	<b>Error! Bookmark not defined.</b>
2.2.5.	Nitrogen .....	12
2.3.	Oxidation and corrosion.....	12
2.4.	Accident Scenarios.....	14
2.5.	Tritium breeding ratio (TBR).....	16
2.6.	Activation.....	20
3.	Novel Zr alloys.....	21
3.1.	Binary Zr systems .....	26
3.1.1.	Zr-Al.....	26
3.1.2.	Zr-Nb.....	29
3.1.3.	Zr-Sn.....	30
3.1.4.	Zr-Be .....	31

3.1.5.	Zr-Ti .....	32
3.1.6.	Zr-Cr .....	32
3.1.7.	Zr-Si .....	33
3.1.8.	Zr-Fe .....	34
3.1.9.	Zr-Mo .....	35
3.1.10.	Zr-V .....	35
3.1.11.	Zr-W .....	36
3.2.	Higher order Zr alloys .....	36
3.2.1.	Zr-Ti-Al-(V) .....	39
3.2.2.	Zr-Al-Sn .....	43
3.2.3.	Zr-Mo-Ti .....	43
3.2.4.	Zr-Nb-Ti .....	44
3.2.5.	Zr-Mo-(Sn) .....	44
3.3.	Comparison of properties .....	45
3.4.	High-entropy alloys .....	47
4.	Summary and Conclusions .....	49
5.	Acknowledgements .....	51
6.	References .....	51

## 1. Introduction

Materials selection and development for fusion reactors is a primary research topic underpinning the progression of fusion technology. Popular candidates for the structural material in the breeder blanket are Fe, V, Cr, or Si based materials. However, recent work has shown that Zr can offer an advantage over these candidates if used as the structural material within the first wall of a DEMO-like reactor, where it was predicted to yield a positive tritium breeding ratio (TBR) relative to an omission of a first wall material [1]. This may offer particularly important advantages for spherical tokamak reactor designs [2,3], where the reduced volume for breeding would mean a higher TBR is harder to obtain.

The development of Zr alloys for in-core nuclear fission applications began ~60 years ago, as a replacement for steel components. Today, examples of Zr alloys that are in regular use include: Zircaloy-2, -4, ZIRLO™, M5®, Zr-2.5 and E110, for fuel assemblies and fuel claddings in light water reactors. Their success is largely due to the small thermal neutron absorption cross-section ( $\sigma_{\text{abs}}$ ) of Zr, 0.185 barns (bn), relative to the majority of elements in other structural materials, which allows for a higher availability of neutrons at thermal energies to sustain criticality of the fission reaction. If other materials

with higher  $\sigma_{\text{abs}}$  are used within the reactor core, the  $^{235}\text{U}$  content in the  $\text{UO}_2$  fuel must be enriched further, which is generally a more financially costly option.

Fusion energy devices, e.g., International Thermonuclear Experimental Reactor (ITER) [4], Demonstration reactor (DEMO) [4,5], and Spherical Tokamak for Energy Production (STEP) [6], present analogous neutron efficiency challenges to fission. To sustain long-term operation, the tritium (T or  $^3_1\text{H}$ ) available for fusion must be replenished. This is to be achieved through the breeding of T during operation via the inelastic scattering of the neutrons produced by the deuterium-tritium (D-T) fusion reaction, with Li, through the following reactions:



Similar to the fission cross-section of  $^{235}\text{U}$ , the T breeding cross-section ( $\sigma_{\text{T}}$ ) of the  $^6_3\text{Li}$  isotope generally increases with decreasing neutron energy (proportional to  $\frac{1}{\sqrt{\text{Energy}}}$ ) and is exothermic, whereas  $\sigma_{\text{T}}$  of the  $^7_3\text{Li}$  is a threshold reaction taking place when neutrons energies are above  $\sim 2$  MeV. Nevertheless, reaction (2) produces T and  $^1_0n$ , which is potentially available for further reaction with  $^6_3\text{Li}$ . Whilst T is produced via both of these reactions in a breeder blanket (the proportion varies depending on the blanket concept), the likelihood of reaction (1) occurring is greater than (2) due to the moderation of neutrons that occurs via elastic scattering with the various components within the reactor (structural material, coolant, multiplier, and reflector) [7]. To exploit these circumstances, enrichment of  $^6_3\text{Li}$  is planned for a majority of designs. However, use of a low thermal neutron absorption cross-section material could be used to the same effect and lead to lower costs and greater design freedom for T breeding in the low energy regime ( $< 1$  MeV).

Figure 1 shows the microscopic neutron cross-sections of T production (n, T) for  $^6_3\text{Li}$ , and non-elastic scattering (n, non) of  $^{56}\text{Fe}$  and  $^{90}\text{Zr}$ . It can be seen that both  $^{90}\text{Zr}$  and  $^{56}\text{Fe}$  exhibit similar resonance behaviour between  $1 \times 10^{-2} - 1$  MeV but below this range, the cross-section of Zr is significantly lower.

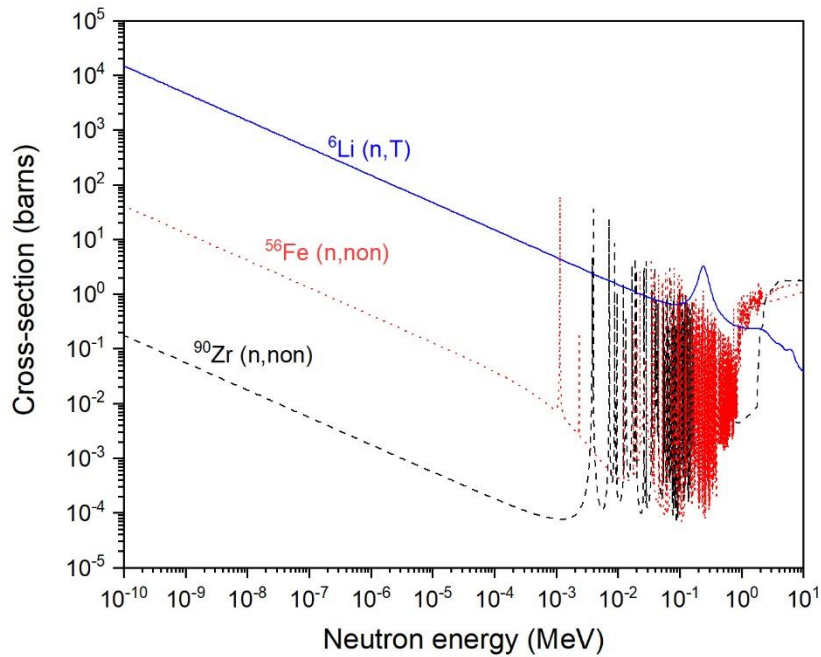


Figure 1. Neutron cross-section for  ${}^6\text{Li}$  breeding T (blue solid line),  ${}^{56}\text{Fe}$  non-elastic scattering (red dotted line),  ${}^{90}\text{Zr}$  non-elastic scattering (black dashed line). Data and references used to construct figure can be found in Ref. [8].

There is a range of proposed designs for future fusion reactors, therefore we must consider a range of conditions that a structural material in the breeder-blanket could be exposed to [5,9]. Some water-cooled fusion reactor designs operate in temperature ranges similar to current light water reactors (300-350°C [10]), and others operate in a higher temperature regime for improved plant thermal efficiency, where leading designs have coolant outlet temperatures in the region of 500 - 700°C [5,9]. Commonly proposed high temperature coolants are: He or H gas, liquid metals such as Li, or molten salts, which will be in direct contact with the coolant pipes composed of the structural material. The structural material will also be in contact with the armour material (e.g. W), the breeder and multiplier material, which are typically Li, Be and/or Pb containing compounds [5,9]. Such alloys will also be exposed to a neutron flux with maximum energies of ~14 MeV [11]. Finally, the mode of operation could be a pulsed mode operation with ~2 h durations and  $\sim 5 \times 10^4$  cycles or quasi-continuous [12].

Of the current designs for the test blanket module (TBM) programme on ITER [13,14], the water-cooled lithium lead (WCLL) breeder blanket concept would employ a temperature range most similar

to those of current fission power plants (280-325°C). At these water-cooled operating temperatures in fission power plants, Zr alloys can feature as the fuel cladding, pressure tubes, fuel channels and fuel spacer grids. The helium-cooled pebble bed (HCPB) breeder blanket concept operates at a higher temperature (300- 500°C) and is another most promising TBM design [15]. It has been shown that Zr as a FW structural material would improve the TBR in this a detached first wall version of the HCPB concept, with excellent mechanical compatibility between the Zr and W as the plasma-facing material due to their similar coefficient of thermal expansion [1]. However, the mechanical behaviour of current commercial Zr at these higher temperatures would likely be unacceptable. Hence, it is pertinent to review novel Zr alloys for higher temperature mechanical stability and highlight key areas for development.

So-far, there has not been any considerable work towards the development of Zr alloys tailored for fusion, and the primary research direction for Zr alloy development has been towards extended operational life in the environment of a light water fission reactor, *viz.* submersion in an aqueous solution at ~300°C [16]. Comprehensive reviews on the effects that neutron radiation has on commercial Zr alloys, in fission reactor conditions, can be found elsewhere [17–19] and will not be discussed in detail here. However, it must be noted that dimensional change via irradiation-induced creep and growth will be a concern for the WCLL design. In fission fuel cladding and pressure tubes, strong texture is created during component fabrication to prevent radial hydrogen-induced cracking. This strong crystallographic anisotropy induces highly directional irradiation-induced growth strains, which is a lifetime-limiting effect. Irradiation-induced growth can be completely absent to very high fluences (> 55 dpa) by quenching to the  $\alpha$ -phase directly from the  $\beta$ -phase and hence randomising the texture, e.g. see section 3.4.1 in Ref [REF Adamson 2019]. Texture randomisation could therefore be considered as a method to limit anisotropic irradiation-induced dimensional change for Zr alloys in the WCLL breeder blanket design. For the HCPB design, at operational temperatures >500 °C, the predominant dimensional change will not be irradiation-induced creep or growth but simply thermal creep [20]. However, it should be noted that the effects of fusion-relevant higher energy flux profiles at these higher temperatures on irradiation-induced dimensional changes have not been investigated for Zr alloys and the mechanical

loading of structural components in the first wall blanket (estimated by Forty and Karditas for a Zr alloy previously [21]) will differ to that of a fuel cladding or assembly [22]. While Forty and Karditas concluded that thermal and irradiation creep would not be life-limiting for a Zr-based water-cooled breeder blanket, no such thermo-mechanical analysis has been performed for a helium-cooled design; commercial Zr alloys experience unacceptably high creep rates ( $>10^{-5} \text{ h}^{-1}$ ) [20] above 500 °C, wherein lies part of the reason for their lack of consideration for fusion. Of further concern is the susceptibility of Zr to H embrittlement. In a review of this latter topic, Forty and Karditsas [23] concluded that H embrittlement of Zr is unlikely to be a life-limiting factor in a fusion environment. However, more work needs to be done to consider the varying sources of H under non-ideal conditions and the effect of pulsed temperature profile of the reactor on delayed hydride cracking. Nevertheless, given the neutronic advantage of Zr, established world-wide extraction/production routes, and their success in fission environments, some consideration should be made for Zr alloys as a structural material in the breeder blanket.

It is therefore the purpose of this review article to consider the high temperature mechanical properties of current Zr alloys and identify the capabilities of advanced Zr alloys, as well as their suitability as structural materials in a fusion environment. Comparisons are made to other current candidate structural materials: EUROFER 97, V-4Cr-4Ti and silicon carbon fibre/silicon carbide composite (SiC<sub>f</sub>/SiC).

## **2. Current Zr alloys**

### **2.1. Material properties**

Currently, ~85% of the globally produced Zr metal is used for nuclear applications (estimated at 6000 t in 2014 [24]). However, this is only a small fraction (<5%) of the total Zr ore extracted annually (~ $10^6$  t), which is used in construction, medical and electronic applications [25]. Natural Zr contains ~4% Hf, which must be removed for nuclear applications due to the high thermal  $\sigma_{\text{abs}}$  of Hf (104.1 bn). Across North America and Europe, nuclear grade Zr is processed by three companies: Compañie European Zirconium Ugine Sandvik, Allegheny Technologies Incorporated, and Western Zirconium. Strip/sheet and tube manufacturing knowledge and capabilities exist globally e.g. at Westinghouse, Framatome, and Sandvik Special Metal. It is therefore plausible that the world supply of Zr could be

upscaled for use in commercial fusion reactors and therefore benefit from the pre-established nuclear supply chain, a feature only Fe alloys currently match.

Table 1 lists example compositions of some popular Zr alloys that have been developed for fission applications. Of these alloys, Zircaloy-2 and -4 have seen the most prevalent use, while M5®, and ZIRLO™ have been the recent successful developments. The design basis for optimised compositions has largely focussed on gaining superior corrosion resistance and reduced H pick-up in aqueous environments.

Table 1. Example compositions (wt.%) of commercial Zr alloys.

<b>Alloy</b>	<b>Sn</b>	<b>Fe</b>	<b>Cr</b>	<b>Ni</b>	<b>Nb</b>	<b>O</b>	<b>Ref.</b>
Zircaloy-1	2.50	-	-	-	-	-	[26]
Zircaloy-2	1.50	0.10	0.10	0.08	-	0.14 <sup>b</sup>	[27]
Zircaloy-3	0.25	0.25	-	-	-	-	[28]
Zircaloy-4	1.50	0.20	0.10	-	-	0.11 <sup>b</sup>	[27]
E110	-	0.05	0.02	0.02	1.10	0.10	[29]
Valloy	-	0.10	1.15	-	-	-	[30]
Ozhenite	0.20	0.10	-	0.10	0.10	-	[31]
Zr-2.5Nb	-	-	-	-	2.50	0.13 <sup>c</sup>	[27]
M5®	0.01	0.05	0.02	-	1.00	0.12	[32]
ZIRLO™	1.00	0.01	-	-	1.00	0.13	[32]
Optimized ZIRLO™	0.67	0.10	-	-	1.00	0.13	[33]

Figure 2 provides a broad comparison of start-of-life thermomechanical properties (thermal conductivity, strength, ductility, toughness, fatigue and creep) measured experimentally for example commercial Zr alloys, compared to three other material families considered for use as structural materials in breeder blanket: EUROFER 97, ODS-EUROFER, V-4Cr-4Ti and, SiC<sub>f</sub>/SiC. It should be noted that the results presented are from a range of studies with differing sample geometries and treatments, therefore care must be taken when comparing exact values. For the purpose of this review only the trends in the data are plotted to provide ease of comparison. Each datapoint used for these trends can be accessed from Ref [8]. In general, it can be seen that Zr alloys underperform in high temperature strength, fracture toughness, room temperature fatigue and creep compared to the other materials. However, they have comparatively good ductility and mid-range thermal conductivity.

At room temperature the strength of Zr-2 is similar to V-4Cr-4Ti, but will soften more dramatically with temperature, and is significantly lower than EUROFER 97, ODS EUROFER and SiC<sub>f</sub>/SiC, between 200 - 800°C. In terms of ductility, Zr and V alloys have relatively high uniform tensile elongations between 0 - 800°C, while SiC<sub>f</sub>/SiC, EUROFER 97, and ODS-EUROFER can present brittle behaviour in this temperature range. The toughness of Zr alloys changes dramatically with H, He and O content; the data for Zr-2 presented in Fig 2(d) is quoted to be 20 wppm H, which is a factor of 2 higher than commercially as-received Zr-2 [34]. A trend of increasing ductile-to-brittle transition temperature (DBTT) is observed for increasing H in some cases [35] but the behaviour can also change dramatically depending on hydride morphology [36]. Nevertheless, commercial Zr alloys have a relatively low fracture toughness above room temperature, intrinsic to its crystal structure [37], making it worse than the other candidate alloys. Similarly, the creep and fatigue performances are worse than the other candidates and are prohibitive factors for use of current Zr alloys as structural components in the blanket region, even in the absence of radiation damage. This is because such components will likely be exposed to cycled thermomechanical loadings, during pulsed mode operation, with maximum operating temperatures higher than the range where commercial Zr alloys can maintain integrity. When including the effects of irradiation, corrosion, cycling, transient conditions, the material design limits become even more restrictive. Previously, EUROFER 97, V-4Cr-4Ti and SiC/SiC have been predicted to have a maximum useful operating temperatures of approximately 550, 650, and 950°C, respectively, when considering irradiation effects [24]. It is clear that for a Zr based alloy to be suitable as a structural component in the breeder blanket, the creep resistance must be improved. While fatigue and creep data are not available for more novel Zr alloys, here the strength is used as a first order approximation assuming that a stronger alloy will display greater creep resistance.

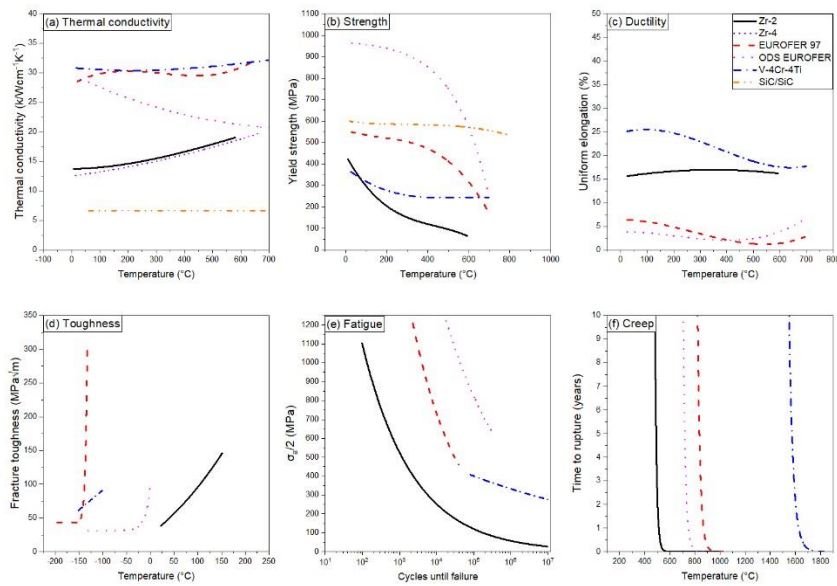


Figure 2. Relative trends in (a) thermal conductivity, (b) yield strengths (flexural strength for SiC<sub>f</sub>/SiC) (c) ductility, (d) toughness, (e) fatigue and (f) creep (50 MPa stress), of Zr, V and Fe based alloys and SiC<sub>f</sub>/SiC, between 0-900°C. The data and literature references used to construct this Figure are accessible from Ref [8].

## 2.2. Manufacturing, joining, and welding

Currently, components made from nuclear grade Zr are first supplied in the form of sheet, plate or tube. These geometries are then manufactured into the desired shapes or welded to other components. Allegheny Technologies Incorporated (ATI), for example, produce Zr sponge and Zr alloys in strip, plate, foil and rod geometries [27]. The main difference between Zr alloy components used in fission and fusion are the thicknesses required i.e. more than a magnitude increase in thickness from 0.5 mm of a Zr-4 fuel cladding [38,39]. The use of Zr alloys, when joining and welding for fusion applications, does offer some advantage if a W is to be used as an armour as both elements have similar thermal expansions [40]. However, a well-documented problem resulting from the manufacturing process is the crystallographic texture introduced in the component that leads to anisotropic properties [41], which would persist in conventional Zr alloy components for fusion applications unless a post-manufacture  $\beta$ -quench heat treatment is included for texture randomisation. Atmospheric contamination, at various stages of Zr alloy processing, is also a known problem and therefore vacuums are needed to reduce these effects [42]. It is not expected additional issues relating to the manufacturing, joining and welding of Zr based components, specific to fusion, will be encountered using current methods.

### 2.3. Effect of impurities (C, H, Li, and N)

Impurities can be introduced to a material at all stages of its life. The susceptibility of the material to impurity pickup and the effects of the impurities on mechanical performance is crucial to the viability of the material. It is this aspect that V based alloys face difficulties as C, N and O impurities, introduced during the fabrication process (at concentrations of 60-300, 70-460 and 150-900 weight parts per million [wppm], respectively [43]), lead to loss of workability [44] and weldability [45] and also lead to precipitation during irradiation [46].

The impurity concentrations of Zircalloys, after fabrication, are detailed in Table 2. Within this section, the perceived sources of additional impurity concentrations, material response and possible issues encountered are discussed based on commercial Zr alloys used in a breeder blanket.

Table 2. Typical start-of-life impurity concentrations in commercial Zr alloys.

Alloy	C (wppm)	H (wppm)	N (wppm)	O (wppm)
Zr-2	270 <sup>a</sup>	25 <sup>a</sup>	80 <sup>a</sup>	1420 <sup>b</sup>
Zr-4	270 <sup>a</sup>	25 <sup>a</sup>	80 <sup>a</sup>	1100 <sup>b</sup>
Zr-2.5Nb	270 <sup>a</sup>	10 <sup>a</sup>	65 <sup>a</sup>	1300 <sup>c</sup>

<sup>a</sup>[27], <sup>b</sup>[47], <sup>c</sup>[48]

#### 2.3.1. Carbon

At high C concentrations (>0.5 wt%) it is known that there is a deleterious effect on the oxidation resistance of Zr alloys. This is because Zr carbides precipitate at the surface and in the bulk of the material and facilitate the diffusion of O into the material [49]. At impurity concentrations in Zr-2.5Nb, a correlation between increasing C content between 40 – 300 wppm and deuterium pickup has also been observed [50].

The only other likely source of additional C content in a Zr alloy is in the form of <sup>14</sup>C, which can be produced by the interaction of fast neutrons with <sup>14</sup>N, via <sup>14</sup>N(n,p)<sup>14</sup>C. The levels that are produced (~1 wppm/yr [29]) are not expected to have a large impact on the behaviour of the material during operation, but would impact on the induced radioactivity in the material [51].

#### 2.3.2. Hydrogen

Zr has a reasonably large H solubility (>0.15 wt%) at elevated temperatures (>300°C). Therefore, during thermal cycling there is an energetic drive for H adsorption and dissolution into the metal at high

temperatures, and subsequent precipitation as brittle hydride phases at low temperatures where H solubility is very low (~1 wppm at 20°C). This can lead to hydride re-orientation and the possibility of delayed hydride cracking. These phenomena are well documented for commercial Zr alloys and an extensive review can be found in Refs [52,53]. The question then shifts to: How much H is available to a structural material in the breeder blanket and what is the H pickup fraction of the material used? In a review by Forty and Karditsas, it is calculated that if the D and T produced by the plasma remains implanted in the armour material, a permeation barrier exists between the breeder and structural material, and there is negligible H pickup from the coolant, then there will be an increase of 27 wppm, due to transmutation, after 5 years of operation [23]. These assumptions are plausible if an effective permeation barrier is developed. Indeed, it was concluded in a review by Davis *et al.*, that at the very least a protective barrier must be in place to prevent the implantation of plasma species to limit H levels in Ti [54]. This notion is further supported by calculations performed by the Japan Atomic Energy Research Institute (JAERI) where it is predicted that for DEMO-like reactors, T permeation from the plasma can be reduced by a factor of  $10^3$ , when the W armour thickness is increased to 1 mm, coated on a low-activation ferritic/martensitic steel, compared to the omission of a first wall armour. However, due to the uncertainty in diffusion rates in the various components within the blanket, it is difficult to place an exact T inventory of each component. It is likely that the increased affinity of Zr for H will translate to a higher degree of trapping of T compared to other candidate materials, as seen with V based materials [55]. Further work should be done to assess the T diffusion rate through different materials and observe the T retention in layered systems where barriers between the T sources and a Zr material exist.

### **2.3.3. Helium**

The introduction of He to a Zr alloy will occur due to  $(n,\alpha)$  transmutations within the material during operation. Unlike many other materials, He does not lead to excessive void formation and swelling in Zr alloys [56]. It has been predicted in the past, that in a DEMO-like reactor, for a Zr alloy in the blanket region, the He concentrations produced via transmutation will not be a life limiting factor [57]. However, if the alloy is subject to continuous He coolant interaction at elevated temperatures and under neutron irradiation, a different behaviour may be observed. Currently, no data exists that would

allow for a reasonable prediction as to the interaction and behaviour, therefore, further experimentation is necessary to investigate whether a He coolant would be compatible with a Zr alloy.

#### **2.3.4. Nitrogen**

Historically, N was responsible for increased aqueous corrosion rate in Zircalloys. This effect was counteracted with additions of Sn [26]. However, the Zr manufacturing process has since been refined to reduce the N contents to concentrations that do not substantially impact the corrosion resistance and therefore additional Sn is not needed. As far as the Authors are aware there is no published mechanistic explanations for Sn counteracting the effect of N.

The influence of N on oxidation of Zr alloys has also been documented. The effects have been studied in the context of “loss of coolant accidents” (LOCA) where it has been shown that the presence of N in steam can lead to increased oxidation rate at high temperatures ( $>600^{\circ}\text{C}$ ) [58]. The mechanism proposed to be responsible for this, is that nitrides are formed between the oxide and Zr metal interface which accelerates oxidation of the metal as the nitrides oxidise two orders of magnitude faster compared to a non-nitrided metal [32].

There is not expected to be a significantly high enough concentration of N to be available in the start-of-life Zr or coolant types for deleterious effects to result in a fusion environment.

#### **2.4. Oxidation**

When Zr-based alloys are exposed to O, various sub-oxides are formed in a concentration gradient from the metal to  $\text{ZrO}_2$  on the surface of the material. The thickness of the  $\text{ZrO}_2$  layer will increase with increasing environmental exposure time and temperature [59]. Initially, this oxidation kinetics follows a parabolic or sub-parabolic relationship and has a protective nature. However, this relationship transitions to a linear oxidation rate, termed “breakaway” oxidation, where degradation of the material occurs [60]. Below  $\sim 300^{\circ}\text{C}$  in air, breakaway oxidation will occur on the order of hundreds of years. However, at temperatures of  $600\text{-}1000^{\circ}\text{C}$  breakaway occurs on the order of hours [61]. At temperatures close to melting, oxidation of Zr in air or steam can lead to catastrophic failures and is a topic of concern for reactor safety [62]. Although fusion reactor breeder blankets will operate in a high vacuum, this rapid failure is of key consideration for accident scenarios and for coolant side exposures; an assessment of the former is made in the following section.

In general, the concentration of impurities, e.g. C, N, H and even O, in the alloy, will increase pre-transition oxidation rate and decrease time to transition [61]. However, the oxidation behaviour is seldom directly proportional with increase in alloying species. Past experimentation on a number of alloying elements (Al, Be, Co, Cu, Cr, Fe, Hf, Mo, Nb, Ni, Pb, Pt, Si, Sn, Ta, Ti, V, and U), in 1, 2 or 4 at.% concentrations, has identified that Be, Ni, and Cu improve oxidation resistance, whereas the others were deleterious or no change was evident to the oxidation behaviour, relative to high purity Zr [61]. However, including elements in lower contents (<1 at.%) often improves the oxidation/corrosion performance [61]. Nevertheless, the oxidation rate of commercial Zr alloys in air and water at mid-range temperatures (~350°C) have reached a stage in which breakaway is not a concern.

## **2.5. Corrosion**

Aqueous corrosion of conventional Zr alloys is a well-documented process, which involves breakdown of the oxide layer and adsorption/ingress of H. A comprehensive review can be found in Ref. [63]. In short, at temperatures that far exceed nominal fission reactor operation ( $\geq 500^\circ\text{C}$ ), aqueous corrosion will be problematic. Therefore, alternative alloys or barrier coatings will need to be utilised in these cases.

For non-aqueous corrosion, the literature is scarce. Regarding liquid metal coolants, Li-Zr alloy interactions have been studied, in the past, as Li is present in the coolant as a pH balance in the form LiOH, in fission reactors. Ingress of Li is known to occur into the Zr oxide layer, which is theorised to increase the porosity and subsequently the corrosion rate [64]. However, the Li-Zr phase diagram predicts complete immiscibility between both species [65], which is supported by the observation that there is no detectable Li concentration in the Zr metal below the oxide layer [64]. It is likely that in a non-aqueous environment, such as if Li or LiPb coolant/breeder is used, that the interaction behaviour with the Zr oxide layer will change significantly. Data of this nature is not available and further work in this area is required.

Much work into liquid metal embrittlement (LME), by corrosion or diffusion controlled intergranular penetration, has been conducted for a range of alloy/metal combinations [66]. However, comprehensive data is lacking for Zr alloy -Li and -Pb combinations. The most relevant work on this

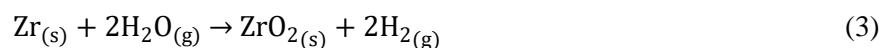
topic is likely unpublished and only mentions can be found [67]. Nevertheless, what is mentioned is that Zr based materials are not particularly susceptible to LME by Li with testing being conducted between 482 - 1000°C [68].

Another aspect that must be considered with exposure of Zr alloys to liquid metal environments is the latter's increased susceptibility to the pickup of impurities. Transfer of material across temperature gradients are typically observed [69], this effect may lead to a heterogenous distribution of impurities within the coolant loop. An assessment of the extent of these effects is needed for Zr alloys and coolants.

In terms of barriers between the structural material/coolant and /breeder, ceramic coatings (e.g. Cr<sub>2</sub>O<sub>3</sub>) are being developed for both fission [70,71] and fusion applications [72]. It is important to note that if a non-aqueous coolant is used (e.g. Li, PbLi, He, CO<sub>2</sub>, FLiBe and FLiNaK), H may still be present as a dissolved impurity or may even be deliberately added as water to improve T extraction. Further, Zr has a high affinity for F and the ZrF<sub>4</sub> formation enthalpy (-4 eV/atom) is significantly more favourable than KF, NaF, LiF, FeF<sub>2</sub> and VF<sub>4</sub> (~-3 eV/atom) [73]. However, Cr has a much lower affinity to F with CrF<sub>6</sub> having a formation enthalpy of -2 eV/atom. Therefore, an effective barrier coating will need to be used regardless of whether aqueous or non-aqueous coolants are used. Moreover, such coatings currently do have promise but further work is still required for industrial applications.

## 2.6. Accident Scenarios

As mentioned, the breakaway oxidation of Zr can lead to catastrophic failure, as evidenced most recently in the Fukushima Daichi accident [74]. This occurs due to the build-up and ignition of H<sub>2</sub> gas resulting from the following reaction:



For a catastrophic explosive reaction to occur, via this mechanism, three conditions must be met:

- A high volume of H<sub>2</sub>O needs to be available for H<sub>2</sub> gas production.
- Sufficiently high temperatures ( $\geq 1200^\circ\text{C}$  [62]) must be reached for rapid oxidation rate.

- Critical gaseous H<sub>2</sub> concentration (15-30 vol.%) in a proportionate layer thickness that allows for flame acceleration and detonation initiation [75].

The reaction rate of Eq (3) is proportional to the temperature; in the fission industry, emergency core cooling acceptance criteria limits peak Zr cladding temperature to 1200°C [62]. In the Fukushima accident, the fuel and control rods were completely melted ( $\geq 2800^\circ\text{C}$ ) 16 h after loss of coolant occurred. These temperatures are well above the step-change in oxidation rate observed at 1580°C for Zr [76]. It is thought that approximately 130 kg of H<sub>2</sub> was ignited during the explosion of Fukushima Unit One after ~25 h [77]. Production of this quantity of H<sub>2</sub> would require the reaction of roughly an order of magnitude larger amount of H<sub>2</sub>O, which is also roughly 1572 m<sup>3</sup> of water under ambient conditions. The combined volume of the coolant system of ITER is an order of magnitude larger than this [78], therefore if a water coolant is used in a fusion power reactor of similar size, there will be a sufficient supply of H<sub>2</sub>O for such volumes of H<sub>2</sub> gas to be produced via oxidation of Zr. However, if a non-aqueous coolant is used, there is not expected to be any other source of H<sub>2</sub>O large enough for this to occur.

A large difference between LOCA accidents in fission [79] and fusion [80] environments is that the latter does not have a continued supply of heat generated by the fuel. Therefore, heat will only be generated from the decay of irradiated structural and breeding material. A worst-case LOCA model of a fusion power plant, in which no back-up cooling systems are engaged and minimal heat removal to the environment occurs, predicts that the maximum temperature within reactor will be the first wall, which could reach ~1000°C after 4 days to a maximum of ~1200°C after 30 days [81]. The latter timeframe is somewhat unrealistic for an accident scenario. However, at these temperatures, the rate of oxidation is on the threshold considered dangerous for Zircalloys [62]. Providing there is a sufficient thermal gradient away from the first wall towards a Zr structural material, and/or there is no exposure of Zr to steam at such temperatures, it is not expected that oxidation of Zr will occur at a sufficient rate for H<sub>2</sub> gas accumulation to occur to a sufficient concentration or volume for a catastrophic event to occur during a fusion power plant LOCA.

## 2.7. Tritium breeding ratio (TBR)

The TBR is the ratio of the rate of T produced during operation (Eqs. 1 and 2), to the rate of T burned in plasma. The feasibility of T breeding depends on both basic physics and engineering issues. It is estimated that a TBR of 1.10 – 1.15, i.e. incorporating a margin exceeding unity, will need to be achieved to safeguard against periods of breeding losses from decay (time between production and use) and/or incomplete recovery of bred T [82].

The TBR when Zr is used as a structural material has previously been calculated by Barrett *et al.* [1]. In their publication it is stated that the calculations were performed on a He-cooled pebble-bed design, however, details of breeder type, structural fraction, and  ${}^6\text{Li}$  enrichment were not provided. Nevertheless, the TBR using Zr, as a structural material in the first wall, was calculated to be higher than without a structural material and to be superior to the other candidates (Cr, Fe, V). Among the other candidates, the relative TBR of V-4Cr-4Ti, ferritic steel and SiC<sub>f</sub>/SiC structural materials have been calculated for differing breeders by Sawan and Abdou [82], where it was shown the V-4Cr-4Ti is calculated to achieve the highest TBR of the three candidates, however, Zr alloys were not considered in parallel and there have been no studies that consider the TBR with Zr as a structural material for the whole breeder blanket.

There are many factors that affect the TBR of a fusion reactor, e.g. breeder material, placement, geometry, multiplier, coolant, and  ${}^6\text{Li}$  enrichment. As a result, there is a significant range in the calculated TBR when varying these conditions. It is therefore not useful to quote or compare the magnitude of the calculated TBR between different models, and so here we have calculated relative comparisons through a normalised TBR using a simplified system using OpenMC [83], see Figure 3. The water cooled lithium lead (WCLL) and helium cooled lithium lead (HCLL) designs were simulated to provide a comparison between designs that would operate at temperatures similar to commercial Zr alloys in fission reactors (305°C) [13,14] and one that operates at higher temperatures (500°C), respectively. Both designs predicted near identical trends in the data therefore only the results for the HCLL design is shown here. The results for the WCLL design can be seen in Fig. A2 in the *Appendix*. For both, the armour material was W coated EUROFER 97, and Pb-Li as the breeding material. The fraction of structural material (EUROFER 97, SiC, V-4Cr-4Ti, and Zr-4) was varied from 0.0 – 0.9,

complimentary to the breeder fraction, which was varied from 1.0 – 0.1, where the TBR at this maximum fraction (i.e. no structural material) is used to normalise the data. The  ${}^6\text{Li}$  enrichment fraction in the breeder was also varied from 0.0 - 1.0 and the results are displayed in Figure 4. Further details of the methodology are provided in the *Appendix*.

From the TBR results in Figure 3, it is predicted that Zr-4 will outperform all other candidates by up to ~0.1 or structural fractions  $\leq 0.8$ . Structural fractions above 0.8 are likely far exceeding the structural fractions that are practicable, as current practical designs include EUROFER 97 in the range of 0.14 – 0.20 material fractions across different breeders [84,85]. Although a TBR increase of 0.1 can certainly be obtained through a variety of methods, such as Li enrichment, redesigning the blanket structure, changing first wall thickness, changing coolant etc. Naturally, each method of increasing the TBR will have associated problems. For example increased  ${}^6\text{Li}$  enrichment will have associated cost and waste, redesigning the structure to have less structural material could cause weaknesses, increasing the breeder volume will also have increased relative costs compared to the structural material. Further, some reactor designs have less freedoms that influence the TBR than others e.g. spherical reactors do not have room for inboard breeding [86], therefore knowledge of additional methods of attaining an increase in TBR is of interest to the community. This, in addition to the existing industry for mass production and machining of Zr based components, places them at an advantage over other candidate materials. It should be noted, however, that a more focused cost-benefit review of the reactor designs that would most benefit from this increased TBR, using Zr, should be made before committing long-term research efforts into the development of a high temperature Zr structural alloy e.g. for reactor designs that are predicted to comfortably meet TBR requirements [87], the use of Zr may not be of benefit. Further, designs that utilise Zr alloys complimentary to other candidate materials should also be considered.

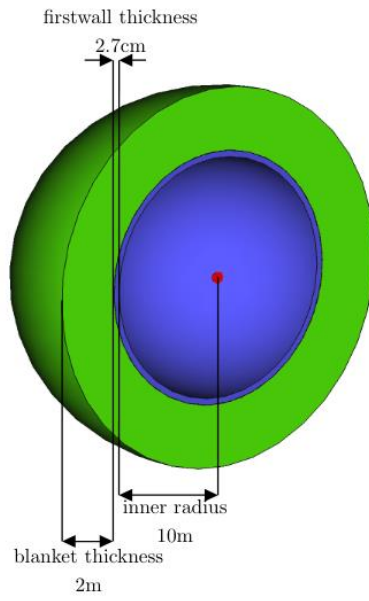


Figure 3. Cross-section of the simple sphere geometry (not to scale) where the breeder blanket (outer sphere), surrounds the first wall (inner circle) and is separated from the neutron point source (middle circle) by a vacuum.

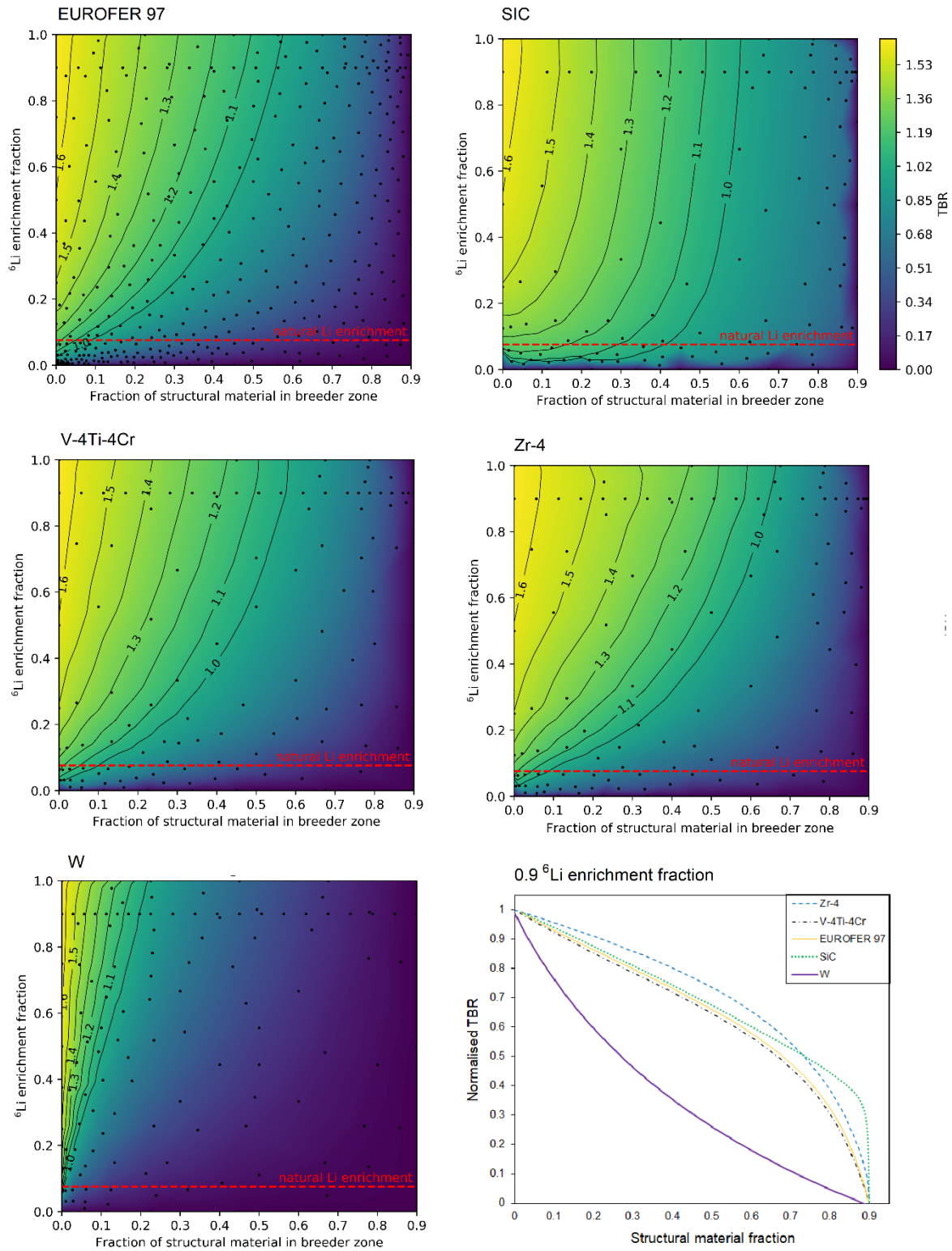


Figure 4. The tritium breeding ratio (intensity scale and numbered solid lines) of each structural material (labelled panels) calculated at discrete points (solid circles) as a function of structural material fraction and  ${}^6\text{Li}$  enrichment fraction. The final panel is a plot of the normalised TBR with 0.9  ${}^6\text{Li}$  enrichment fraction.

## 2.8. Activation

The activity of the majority of elements in the periodic table, 100 years succeeding 2 full power years in a DEMO-like reactor (an approximation of the lifetime exposure of in-vessel components), has been assessed for this review in a similar manner to a previous publication [51]. Each element assessed has been coloured according to their resultant activity, see Figure 5. Of the base elements that constitute the currently considered alloys within this report, the activities of C, Fe, Si and V are within the range of  $10^6$ - $10^7$  Bq·kg<sup>-1</sup>, and Zr is more active at  $\sim 10^8$  Bq·kg<sup>-1</sup>. Of the minor metallic alloying elements, Co, Cu, Mo, Nb, Ni and Sn are even higher in activity ranging from  $10^9$ - $10^{11}$  Bq·kg<sup>-1</sup>. Notwithstanding that Zr is the more active base element, the “cooling” over time is considerably influenced by alloying additions and impurities. For this review, FISPACT-II was used with the same method as Ref. [88] to calculate the activity over time of alloyed examples of the four materials Zr-4, V-4-4, SiC, EUROFER 97, and an armour material W, see Figure 6. We show that over 100 years the relative activities change considerably. Interestingly, after this time period, it is only SiC, V-4-4, and W that fall below the UK low-level waste (LLW) limit ( $1.2 \times 10^7$  Bq·kg<sup>-1</sup>); a design goal pursued by the European fusion research community [89,90]. Nevertheless, Zr-4 presents the highest activity of the candidates. In light of these results, it may be that the activity of such a component cannot meet the aforementioned 100 year LLW goal, while including Zr as a majority element, and that the approach should shift to pursuing an “as low as reasonably practicable (ALARP)” [91] design goal. This may be justified via the necessity to achieve a positive TBR in specific reactor designs. However, further cost-benefit analysis is required.

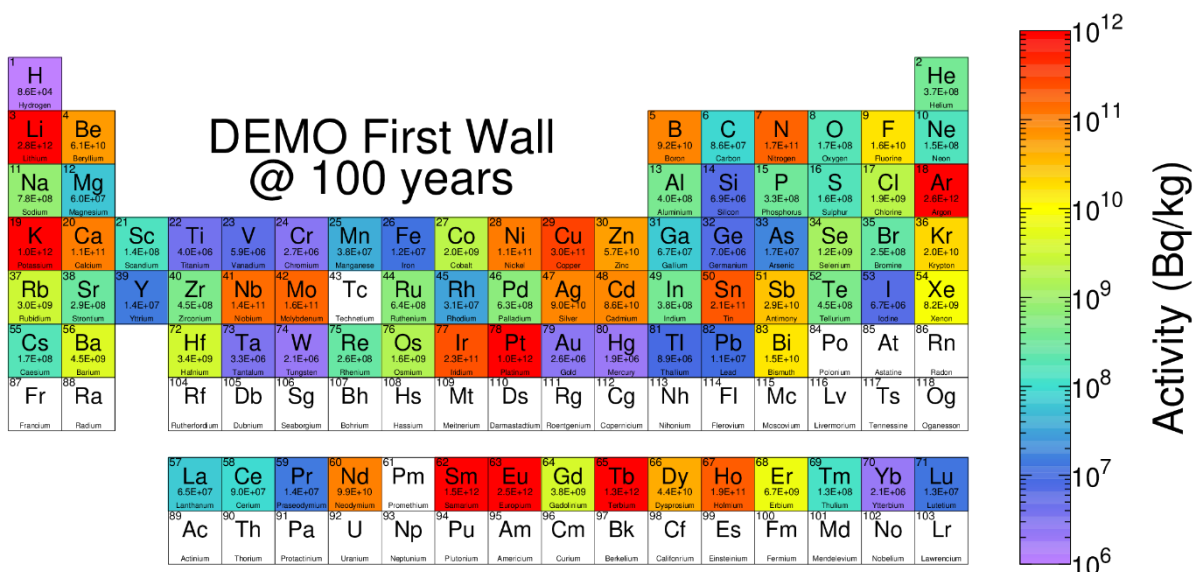


Figure 5. Periodic table showing the total becquerel activity from each element after 100 years of decay cooling following a 2 full power year irradiation in a DEMO firstwall environment. The colour of each element reflects the activity according to the Bq·kg<sup>-1</sup> legend, but the absolute values are also given beneath each element symbol.

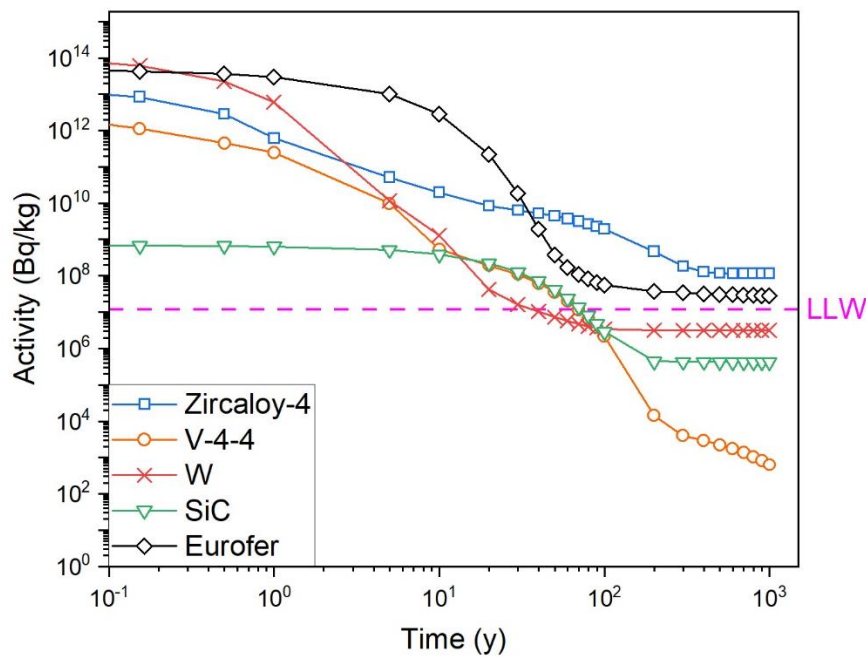


Figure 6. Activity of Zr-4 (blue squares), V-4-4 (orange circles), W (red crosses), SiC (green triangles) and EUROFER 97 (black diamonds) as a function of time. The UK low level waste limit (LLW) is denoted by a horizontal fuchsia dashed line.

### 3. Novel Zr alloys

In this section we review opportunities for novel Zr alloys with higher temperature capabilities than conventional Zr alloys, specifically: binary systems of Zr-X, where X refers to elements Al, Be, Cr, Fe, Hf, Mg, Mo, Nb, Ni, Os, Pd, Re, Ru, Sc, Si, Sn, Ta, Ti, V, W and Y, and higher order (3+ element) systems. Microstructure and mechanical property data pertaining to many of these systems is scarce and irradiation data is scarcer. Studies that go beyond that of the initial phase diagram development for non-amorphous Zr rich binary mixtures have been identified and summarised in Table 3. A tally (sum of check boxes) of the type of data is provided as a “score” to quantify the breadth of

data available for each system. Systems with scores  $\geq 2$ , have been discussed in the following subsections.

It is recognised that there are many different breeder designs proposed for DEMO-like fusion reactors. Here we do not provide an assessment for a specific design, rather, we assume the operating temperature ranges from room temperature (RT) to 700°C to cover a range of designs [92]. Further, work in the context of the Zr alloy to be used as a structural component is reviewed but it is recognised that there are also works that focus on Zr as a T storage material, e.g. Zr61Co39 (wt.%) [93,94], which is not reviewed here. Comments on activity and thermal neutron absorption cross-sections refer to data presented in Figure 5 and Figure 7, respectively. Measures of “good” strength and ductility are relative to conventional Zr alloys (~400 MPa), and the minimum uniform elongation of a material to be considered ductile (5%) [95], respectively, at room temperature. Assessments of activity are made from Figure 5, i.e. 100 years after operation in a DEMO-like reactor and comments are made relative to Zr. Finally, the available mechanical property data, and calculated thermal neutron cross-sections for the specific compositions tested in each system, are compared in the section proceeding the binary and higher order systems.

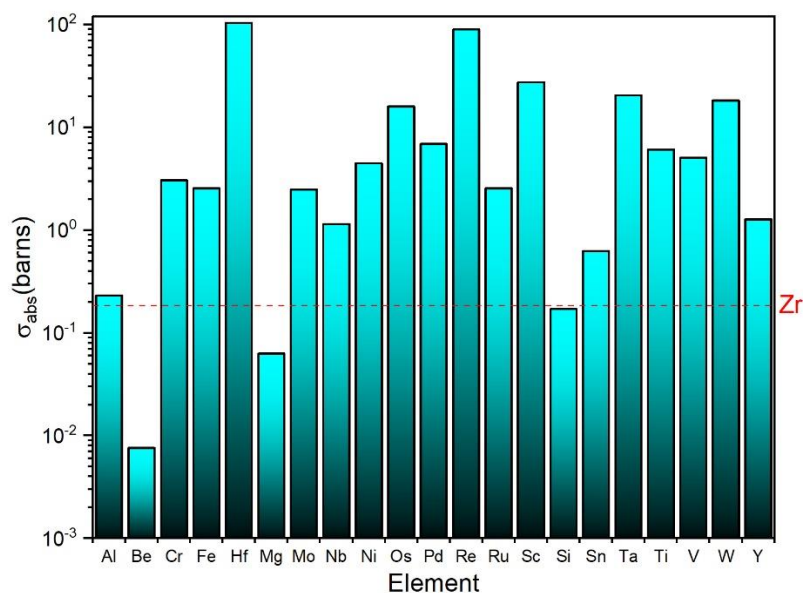


Figure 7. Microscopic thermal neutron absorption cross-sections (y-axis) of each labelled element (x-axis). Values plotted from Ref. [96] for neutron energies of  $2.53 \times 10^{-8}$  MeV.

1 Table 3. Checklist and tally of the type of data identified within this review to be available within the scientific literature for each Zr-X binary system where X is the alloying  
 2 element. RT,  $\sigma$  and  $\epsilon$  refer to room temperature, stress, and strain, respectively.

Alloying element	Microstructure			Mechanical properties			Score	<i>Pros</i>	<i>Cons</i>	Future work
	As-cast	Heat treated 500-700°C	Heat treated >700°C	RT		>RT				
				$\sigma$ vs $\epsilon$	Hardness	$\sigma$ vs $\epsilon$				
Al	✓ [97]	✓ [98]	✓ [98-100]	✓ [98,99,101]	✓ [97]	✓ [98,99,102]	6	<ul style="list-style-type: none"> <li>• Low thermal neutron absorption cross-section.</li> <li>• Precipitate and solid solution strengthening.</li> <li>• Good ductility.</li> <li>• Good creep resistance.</li> <li>• Similar level of activity to Zr (<math>\sim 4 \times 10^8</math> Bq·kg<sup>-1</sup>).</li> </ul>	<ul style="list-style-type: none"> <li>• Lack of ductility when surface flaws are present. Susceptible to corrosion in aqueous environments.</li> </ul>	<ul style="list-style-type: none"> <li>• Strengthen compositions that are ductile at room temperature (<math>\leq 7.8</math> wt.% Al).</li> <li>• Increase ductility of the stronger more creep resistant compositions (<math>&gt; 7.8</math> wt.%). The effect of alloying additional species is the most obvious avenue of exploration.</li> </ul>
Nb	✓ [103]	✓ [104,105]	✓ [106]	✓ [103,106]		✓ [107]	5	<ul style="list-style-type: none"> <li>• Relatively low thermal neutron absorption cross-section. Can present good room temperature strength and ductility due to dual <math>\alpha</math>-(Zr,Nb) + <math>\beta</math>-(Zr,Nb) phase morphology.</li> </ul>	<ul style="list-style-type: none"> <li>• Between 500-700°C segregation will occur.</li> <li>• Nb has a significantly higher activity (<math>10^{11}</math> Bq·kg<sup>-1</sup>).</li> </ul>	<ul style="list-style-type: none"> <li>• Addition of Nb in concentrations <math>&lt; 2.5</math> wt.% that dissolve into the <math>\alpha</math>-Zr phase for solid solution strengthening or mixing of other elements that form better precipitate morphologies with Nb.</li> </ul>
Sn		✓ [108]	✓ [108,109]	✓ [110]	✓ [108]	✓ [110]	5	<ul style="list-style-type: none"> <li>• Low thermal neutron absorption cross-section. Increased creep resistance.</li> </ul>	<ul style="list-style-type: none"> <li>• Inadequate strength as binary alloy for structural applications at 500-700°C.</li> <li>• Sn has a significantly higher activity (<math>\sim 2 \times 10^{11}</math> Bq·kg<sup>-1</sup>).</li> </ul>	<ul style="list-style-type: none"> <li>• Alloying of additional species is required to achieve higher strengths.</li> </ul>
Be	✓ [111]	✓ [112]	✓ [112]	✓ [112]			4	<ul style="list-style-type: none"> <li>• Low thermal neutron absorption cross-section.</li> <li>• The Be<sub>2</sub>Zr precipitate is not an embrittling phase and provides good room temperature mechanical properties.</li> <li>• Improves corrosion resistance.</li> </ul>	<ul style="list-style-type: none"> <li>• Toxicity of Be compounds</li> <li>• Low natural abundance</li> <li>• Be has a significantly high activity (<math>9 \times 10^{10}</math> Bq·kg<sup>-1</sup>)</li> </ul>	<ul style="list-style-type: none"> <li>• The mechanical properties at elevated temperatures need to be examined.</li> </ul>
Ti	✓ [113]		✓ [113,114]	✓ [113,115]			3	<ul style="list-style-type: none"> <li>• Allows for tailoring of <math>\alpha \rightarrow \beta</math> transition temperature.</li> <li>• Good room temperature mechanical properties.</li> </ul>	<ul style="list-style-type: none"> <li>• Relatively higher thermal neutron absorption cross-section.</li> </ul>	<ul style="list-style-type: none"> <li>• Investigation of <math>\beta</math> phase retention during ageing and mechanical properties at elevated temperature.</li> </ul>

								<ul style="list-style-type: none"> <li>• lower activation (<math>4 \times 10^6 \text{ Bq} \cdot \text{kg}^{-1}</math>)</li> </ul>		
Cr		✓ [116]	✓ [116,117]	✓ [116,117]			3	<ul style="list-style-type: none"> <li>• Good precipitate strengthening.</li> <li>• Cr will have a significantly lower activity to Zr (<math>10^6 \text{ Bq} \cdot \text{kg}^{-1}</math>).</li> <li>• Can form stable oxide layer.</li> </ul>	<ul style="list-style-type: none"> <li>• Alloying of Cr limited by higher thermal neutron absorption cross-section.</li> </ul>	<ul style="list-style-type: none"> <li>• Ageing studies and mechanical property experiments are required.</li> </ul>
Si	✓ [118]		✓ [119]	✓ [118]			3	<ul style="list-style-type: none"> <li>• Low thermal neutron absorption cross-section.</li> <li>• Good precipitation strengthening with maintenance of ductility.</li> <li>• Potential for creep resistance.</li> <li>• Lower activity Zr (<math>\sim 10^7 \text{ Bq} \cdot \text{kg}^{-1}</math>)</li> </ul>	<ul style="list-style-type: none"> <li>• Will likely form additional embrittling silicides when alloyed with other species.</li> </ul>	<ul style="list-style-type: none"> <li>• Theoretical work to predict resultant silicides due to alloying with other species should also be done.</li> <li>• Annealing experiments are needed to determine if the <math>\text{Zr}_3\text{Si}</math> silicide forms at 500-700°C.</li> <li>• Mechanical properties at temperature will also need to be evaluated.</li> </ul>
Fe	✓ [116]	✓ [116]	✓ [116]				3	<ul style="list-style-type: none"> <li>• Opportunity for precipitate strengthening.</li> <li>• Lower activity (<math>\sim 10^7 \text{ Bq} \cdot \text{kg}^{-1}</math>).</li> </ul>	<ul style="list-style-type: none"> <li>• Fe may segregate and cause embrittlement due to fast diffusion in Zr.</li> </ul>	<ul style="list-style-type: none"> <li>• Ageing studies are required to identify the stability of the <math>\text{Zr}_2\text{Fe}</math> phase. Annealing studies of polycrystalline Zr-Fe alloys are required to determine resultant microstructures.</li> </ul>
Mo	✓ [120]	✓ [121]				✓ [121]	3	<ul style="list-style-type: none"> <li>• May provide resistance to H retention and corrosion resistance in water.</li> <li>• High melting temperature.</li> </ul>	<ul style="list-style-type: none"> <li>• Higher thermal neutron absorption cross-section.</li> <li>• Low strength at 400°C.</li> <li>• Significantly higher activity (<math>10^{11} \text{ Bq} \cdot \text{kg}^{-1}</math>)</li> </ul>	<ul style="list-style-type: none"> <li>• Microstructural and mechanical property testing with alloying of additional species.</li> </ul>
V			✓ [122]	✓ [122]			2	<ul style="list-style-type: none"> <li>• Could be used for precipitate strengthening.</li> <li>• V has a lower activity (<math>10^7 \text{ Bq} \cdot \text{kg}^{-1}</math>)</li> </ul>	<ul style="list-style-type: none"> <li>• Alloying of V limited by its higher thermal neutron absorption cross-section.</li> </ul>	<ul style="list-style-type: none"> <li>• Examine the microstructures and mechanical properties of components aged between 500-700°C.</li> </ul>
W			✓ [123]	✓ [123]			2	<ul style="list-style-type: none"> <li>• Very high melting temperature</li> <li>• High strengths</li> <li>• Lower activity (<math>10^7 \text{ Bq} \cdot \text{kg}^{-1}</math>)</li> </ul>	<ul style="list-style-type: none"> <li>• Very high thermal neutron absorption cross-section.</li> <li>• Difficult to alloy and can produce inhomogeneous, brittle microstructures.</li> </ul>	<ul style="list-style-type: none"> <li>• Investigation of methods that allow for better homogenisation of microstructure e.g. magnetron sputtering, mechanical alloying, or additive manufacturing.</li> </ul>
Hf			✓ [124]				1			

Os		✓ [125]	✓ [125]				1	
Ru		✓ [126]					1	
Re			✓ [127]				1	
Y			✓ [128]				1	
Mg							0	
Ni							0	
Pd							0	
Sc							0	
Ta							0	

3

### 3.1. Binary Zr systems

#### 3.1.1. Zr-Al

The solubility of Al in Zr is  $\sim 1$  at.% in the  $\alpha$ -phase at temperatures  $\leq 600^\circ\text{C}$ . The intermetallic compound,  $\text{Zr}_3\text{Al}$  (cubic  $L1_2$ ), exists immediately outside these bounds [129]. The  $\text{Zr}_3\text{Al}$  intermetallic is relatively ductile due to the five independent  $\{111\}\{110\}$  slip systems of the  $L1_2$  structure [98] and has been demonstrated to exhibit room temperature ductility [101]. A significant body of work on mixtures close to  $3\text{Zr}:1\text{Al}$  has been performed, pioneered by Schulson *et al.* in the 1970s, for use as a structural material in nuclear fission reactors [98].  $\text{Zr}_3\text{Al}$  forms via peritectoid transformation at  $\sim 1020^\circ\text{C}$  between  $\beta\text{-Zr}$  and  $\text{Zr}_2\text{Al}$  (tetragonal  $B8_2$ ). Due to the lack of solubility of excess Zr or Al in the compound, monolithic samples have not been studied to date, and instead  $\text{Zr}_2\text{Al}$  and  $\alpha\text{-Zr}$  are also present in the microstructure, where they are observed at intra and intergranular locations, respectively. The mixing of Al in excess of 7.8 wt.% Al increases the phase fraction of  $\text{Zr}_2\text{Al}$  ( $>10$  vol.%) and decreases the room temperature elongation. Conversely, a deficiency of Al below 7.8 wt.% will decrease the  $\text{Zr}_2\text{Al}$  phase fraction and increase ductility [102]. It is hypothesised that the morphology of the intergranular region, i.e. solid solution of  $\alpha\text{-(Zr,Al)}$ , contributes to the ductility of the material; analogous to the  $\text{Ni}_3\text{Al}$  intermetallic that can be made ductile at room temperature by B doping, which is thought to lead to the formation of a disordered face centred cubic (FCC) phase at the grain boundary [130]. Therefore, in  $\text{Zr}_3\text{Al}$ , a decrease in Al content will also promote grain boundary  $\alpha\text{-(Zr,Al)}$  formation increasing ductility.

The extent of ductility of this material is highly dependent on the surface state. For example, a polished material with Al concentration of 8.6% can exhibit room temperature elongation of  $\sim 30\%$  at failure, however, if stress concentrations such as machining marks or abrasions exist, the total elongation has been measured to be  $\leq 5\%$  [99,131]. This notch sensitivity may be a limiting factor for the use of such a material in a large-scale industrial setting, where surface state is difficult to control. As-such for the purposes of this review, the material is assumed not to be in a polished state.

For long term ( $\geq 1000$  h) operation at elevated temperatures ( $500\text{-}700^\circ\text{C}$ ) it is possible that grain growth will occur. A study of the mechanical properties as a function of grain size and temperature has been performed for 8.9 wt.% Al samples [101]. After ageing for 1000 h between  $800\text{-}1000^\circ\text{C}$ , a

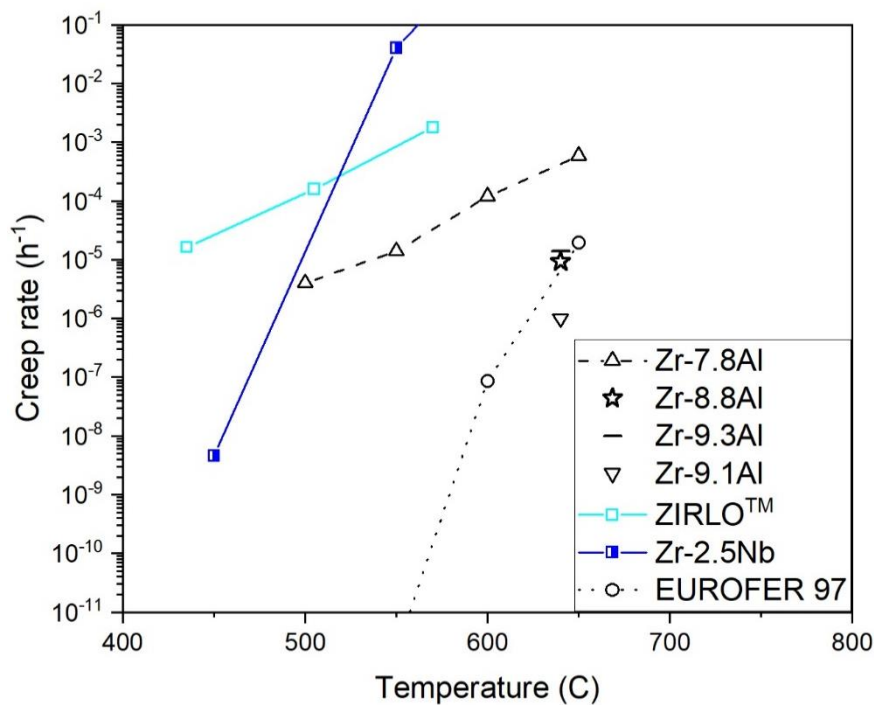
32 decrease in room temperature yield strength from ~650 MPa to 180 MPa was measured. This  
33 corresponded to grains sizes increasing from 1.6  $\mu\text{m}$  to 65.0  $\mu\text{m}$ . This extent of softening is likely too  
34 severe for the structural requirements in a breeder blanket. However, additional work has shown that  
35 some degree of resistance to grain growth can occur between RT and 600°C where samples maintained  
36 grainsize at ~29  $\mu\text{m}$  [98], although the heating rate of the samples was not explicitly stated. This  
37 resistance was attributed to the Kear-Wiltsdorf type dislocation mechanism, also observed in other  $\text{L1}_2$   
38 materials [98]. It follows that if resistance to grain coarsening at ageing temperatures between 500-  
39 700°C can be demonstrated during long term ageing treatments, it is plausible that this material could  
40 meet the strength requirements of a structural material in the breeder blanket.

41 Irradiations using electrons, light/heavy ions and neutrons have been performed on the  $\text{Zr}_3\text{Al}$   
42 precipitate from RT to 400°C [132]. It is observed that the structure disorders initially and then  
43 amorphises at higher fluences (equivalent of >1.4 dpa) between the aforementioned temperature range.  
44 There is an irradiation-induced swelling ( $\leq 5$  vol.%) associated with this disorder but it is inversely  
45 proportional to irradiation temperature. Post-irradiation annealing at 575°C for 1 h allows for a  
46 complete recovery of damage [133].

47 In a study of  $\alpha$ -Zr alloys with lower Al concentrations (3 – 15 at.%) [100], samples were hot-  
48 rolled at 920°C then air cooled. Single-phase  $\alpha$ -Zr microstructures were observed until Al was included  
49 in concentrations  $\leq 9$  at.%. Above 9 at.%, precipitation of  $\text{Zr}_3\text{Al}$  occurred. It is assumed that the cooling  
50 rate of the samples did not allow for precipitation below <9 at.% Al, an assumption supported by a  
51 separate study that observes  $\text{Zr}_3\text{Al}$  precipitation in a 6 at.% sample after annealing for 4 h at  
52 800°C [134]. Nevertheless, a significant strengthening effect was demonstrated, with a maximum  
53 measured yield stress of ~1200 MPa. Furthermore, a good retention of ductility is observed for  
54 compositions with  $\leq 12$  at.% Al with ~8% total elongation.

55 The steady state tensile creep rates of compositions close to 3Zr:1Al have been measured at  
56 various temperatures and stresses [135]. Figure 8 provides a comparison between these creep rates and  
57 that of EUROFER 97 [136], ZIRLO<sup>TM</sup> [137], and Zr-2.5Nb [138], extrapolated to applied stresses of

58 70 MPa, from past experimental data. It should be noted that there are differences in geometries and  
 59 test conditions between the different studies therefore some error may be associated in the  
 60 comparisons. Nevertheless, for the Zr-Al compositions with 6.8-7.8 wt.% Al, the reported thermal  
 61 creep rates an improvement relative to ZIRLO™ and Zr-2.5Nb, and sufficiently low for use at  
 62 temperatures  $\leq 550^\circ\text{C}$ . The thermal creep rate was measured to decrease by an order of magnitude for  
 63 compositions with 8.5-9.3 wt.% Al and for a sample with 8.8 wt.% Al, a creep rate of  $9.3 \times 10^{-6} \text{ hr}^{-1}$   
 64 was measured for a stress of 70 MPa at  $640^\circ\text{C}$ . Indeed, when Al is included between 8.8 – 9.1 wt.%  
 65 the creep rate is comparable to EUROFER 97 for temperatures  $\sim 650^\circ\text{C}$ . However, as mentioned  
 66 previously, there are issues with the ductilities of samples with Al contents in this range, which may  
 67 be a prohibitive factor for machining of components suitable for a breeder module.



76 role in corrosion resistance against Pb coolants through the formation of a  $\text{Al}_2\text{O}_3$  scale in other  
77 alloys [141]. However, Zr has a higher activity with O than Al and is likely to take precedence to form  
78  $\text{ZrO}_2$ , as observed in the past [142].

### 79 **3.1.2. Zr-Nb**

80 Niobium is a common alloying addition to Zr in 2.5 wt.% contributions to form the Zr-2.5Nb  
81 alloy, which is popularly used in Canadian nuclear power plants [143] and is also under consideration  
82 for biomedical applications [144]. The attractiveness of this system is the duplex  $\alpha$ -(Zr,Nb) +  $\beta$ -(Zr,Nb)  
83 forming region between 615 - 970°C, which gives rise to a good combination of strength/ductility  
84 (~800 MPa/~14% uniform elongation, respectively, at room temperature [143]), grain size and  
85 microstructure control, as well as good corrosion/oxidation resistance in light water reactor  
86 environments.

87 For fission applications, Zr-2.5Nb tubes are traditionally extruded at 815°C, cold-worked 27%,  
88 and stress relieved at 400°C for 24 h. In this state, a metastable network of  $\beta$ -Zr filaments surround  
89 elongated grains of  $\alpha$ -Zr. Between 400 - 700°C, the Zr content of the  $\beta$  phase has been observed to  
90 reduce with ageing time. The maximum time the Zr rich  $\beta$ -phase was found to be stable was 1000 h  
91 [105]. Further, the  $\beta$ -phase will be composed of ~95 wt.% Nb after  $10^4$  h of ageing, and between 400-  
92 500°C  $\omega$ -Zr (metastable hexagonal [145]) is observed to form within hours of ageing [105].

93 For operating temperatures between 500-700°C the alloy will be outside of the  
94  $\alpha$ (Nb,Zr)+ $\beta$ (Nb,Zr) forming region. Instead, segregation will occur where body centred cubic (BCC)  
95 Nb precipitates decorate  $\alpha$ -Zr grain boundaries [104,146]. It is therefore not predicted that Zr-2.5Nb  
96 will retain its room temperature ductility after long term operation at temperatures relevant to a breeder  
97 blanket.

98 Evaluation of the mechanical properties of Zr-2.5Nb has been conducted between 20-1200°C with  
99 a hold time at each temperature of 3-5 min. A sharp decrease in yield strength was observed after  
100 550°C accompanied by a drastic increase in elongation attributed to the manifestation of superplasticity  
101 [107].

102 M5® is also an example of a commercial Zr-1.0Nb (wt.%) alloy developed for oxidation  
103 resistance and reduced H pickup in light water reactors. There is a notable trend in reduction of Sn and  
104 retention or increase in O to improve corrosion resistance in commercial Zr alloys[147]. The effect of  
105 O content (0.14-4.00 wt.%), in M5® and Zr-4, on the mechanical properties has been observed to  
106 stabilise the  $\alpha$  phase to higher temperatures but embrittle the alloys at RT, at >0.50 wt.% concentrations  
107 [148].

108 Tensile hoop tests have been performed on M5® cladding irradiated for five and six annual cycles  
109 (i.e. fuel burnup of 60-75 GWd·tU<sup>-1</sup>) at temperatures between 250-800°C [149]. It was observed that  
110 the yield strength of M5® decreased linearly with temperature. M5® also displayed a lower yield  
111 strength than Zr-4 between 250-600°C where it decreased from 500-200 MPa. However, between 600-  
112 700°C the yield strength was quite similar to Zr-4 (250-150 MPa). The uniform elongation of M5®  
113 was recorded to be ~1% between 250-450°C but a lot larger at higher temperatures (4.2-6.4% at 600°C  
114 and 8% at 700 °C) for a high strain rate of 1 s<sup>-1</sup>. It should be noted that the heating rate of these tests  
115 were also quite high (200°C·s<sup>-1</sup>) therefore these results are not indicative of samples in their equilibrium  
116 microstructures at these temperatures.

117 It is difficult to translate tensile hoop test results with high strain/heating rates to a prediction of  
118 performance of such alloys in a breeder blanket environment. The following points may be applicable:

- 119 1. The irradiated mechanical performance of M5® is not markedly different from Zr-4 and likely  
120 unsuitable for a breeder blanket material due to high thermal creep rates.
- 121 2. The addition of Nb and/or O may be a more interesting avenue to explore for resistance of H  
122 pickup.

### 123 **3.1.3. Zr-Sn**

124 Tin is a common addition to Zircalloys to increase the creep resistance, stabilise  $\alpha$ -Zr, and control  
125 grain size during processing. However, its addition has been shown to reduce corrosion resistance  
126 [150]. It is measured to be soluble in the  $\alpha$ -Zr matrix up to 5 at.% at 600°C. Outside these bounds the

127 phase diagram predicts a cubic  $Zr_4Sn$  intermetallic to form, which can exist in an off stoichiometric  
128  $Zr_3Sn$  composition [151].

129 Tin is hypothesised to increase the creep resistance of Zr alloys through mechanisms such as:  
130 increase in stress field around Sn (due to the difference in atomic radii) restricting the gliding of  
131 dislocations and diffusion of vacancies and lowering of stacking fault energy [152]. Limited studies  
132 on pure Zr-Sn binary systems that examine the mechanical properties exist in the open literature,  
133 however, various investigations into the microstructure exist [108–110,151]. The tensile properties of  
134  $\beta$ -quenched and tempered martensitic alloys with 2 – 7 at.% Sn has been investigated [110]. The  
135 elongation was not measured to be proportional to Sn content and ranged from 5 – 15% at room  
136 temperature. The yield strengths ~250 MPa are seemingly independent of Sn content at room  
137 temperature. The microstructural analysis revealed precipitation and unidentified black spots in all  
138 samples, which is not predicted from the phase diagram for those with  $\leq 5$  at.% Sn. Therefore, these  
139 results may not be indicative of the binary systems at equilibrium.

#### 140 **3.1.4. Zr-Be**

141 Beryllium is an element that has been considered for use as a first wall material for fusion power  
142 reactors due to its low atomic mass, high melting temperature and neutron transparency [153]. It is  
143 also a prime candidate for use as a neutron multiplier [154]. Be does not form a solid solution with Zr  
144 below 820°C, instead it forms a  $Be_2Zr$  intermetallic compound [155] which is an ordered hexagonally  
145 close packed (HCP) structure [156]. The mechanical properties of mixtures with 2.5 – 9.3 at.% Be  
146 have been studied [111]. As anticipated, the microstructure consisted of  $\alpha$ -Zr and  $Be_2Zr$  at all  
147 concentrations, where the latter is observed to form at the grain boundaries, see Figure 9. A reasonable  
148 trade-off between increase in strength (672 – 892 MPa) and decrease in ductility (14 – 7% total  
149 elongation) was measured over this Be range. Additional experiments were performed on the 5 at.%  
150 Be sample where it was hot-rolled and then vacuum annealed at multiple temperatures between 600 –  
151 850°C for 2 h. A decrease in strength from 786 MPa to 600 MPa, and increase in elongation from 12%  
152 to 17% is observed due to the increase in  $\alpha$ -Zr recrystallisation fraction, grain size, and decrease in  
153 dislocation density [112].

154 It is worth noting that Be has been identified as one of the few elements that increases the  
155 oxidation resistance of pure Zr when alloyed in larger quantities (1, 2 or 4 wt.%) [139].



156

157 Figure 9. Scanning electron microscopy (SEM) micrograph of Zr-5Be (at.%) alloy hot rolled and annealed at  
158 850°C for 2 h taken from Ref [112].

### 159 3.1.5. Zr-Ti

160 Titanium and Zr are mutually soluble with each other and the  $\alpha \rightarrow \beta$  transition temperature is at  
161 its lowest ( $\sim 600^\circ\text{C}$ ) when they are alloyed in equal atomic ratios [157]. A number of studies of binary  
162 alloys with 10 – 50 at.% Ti have been performed, however, these focus on room temperature  
163 applications with  $\beta$  phase retention, and the samples are in a quenched state from the  $\beta$  forming region  
164 ( $\geq 900^\circ\text{C}$ ) [113,115,158,159]. For a structural material operating in the 500 – 700°C region, a single  $\beta$   
165 phase is unstable and a high portion  $\alpha$  phase will likely transform. One study of a 50 at.% Ti alloy  
166 provides results pertaining to samples quenched from 620°C and 750°C [160], which is likely most  
167 applicable to a breeder blanket. At room temperature, only  $\alpha'$ -phase ( $\beta$  transformed  $\alpha$ ) was observed,  
168 and the room temperature mechanical properties were measured to be 800-1100 MPa ultimate tensile  
169 strength (UTS) with 4-7% elongation.

### 170 3.1.6. Zr-Cr

171 Chromium is a common addition in Zircalloys and was initially included as it was found to  
172 enhance corrosion resistance and provide strength [16]. However, the solubility of Cr in Zr is very low  
173 below  $\sim 700^\circ\text{C}$  where the  $\text{ZrCr}_2$  C15 Laves phase will form at equilibrium [161]. The C15 Laves phase  
174 is a relatively strong but brittle intermetallic compound [162].  $\text{Zr}(\text{Cr,Fe})_2$  intermetallics of the same  
175 structure are observed to amorphise at RT to 300°C and dissolve between 300 to 400°C under neutron  
176 irradiation due to radiation enhanced diffusion effects [163].

177 A study of the mechanical properties of arc melted then hot-rolled (870°C) Zr with 0.5 – 3.0 at.%  
178 Cr has been performed [117]. Relatively high room temperature strengths were achieved 966 –  
179 1270 MPa with associated 12.6 – 6.0% elongation. Further, annealing experiments were carried out  
180 on a 1.8 at.% Cr sample at 550°C, 650°C and 750°C for 1 h, then air cooled [116]. Significant  
181 improvements to the ductility were achieved (16 – 18% from 8.8% elongation) accompanied by  
182 decreases in strength (818 – 991 MPa from 1118 MPa) due to coarsening of grains and reduction in  
183 dislocation density.

### 184 **3.1.7. Zr-Si**

185 Silicon forms a range of complex metallic silicides that are strong but brittle intermetallic phases.  
186 Some are widely considered for high temperature structural applications [164], including neutron  
187 reflector components in fast reactors [119]. The Zr-Si phase diagram predicts the formation of Zr<sub>3</sub>Si,  
188 a tetragonal intermetallic, when the temperature and Si concentration is <1571°C and <15 at.%,  
189 respectively [165]. However, a study on an 8.8 at.% mixture did not contain the Zr<sub>3</sub>Si phase in the as-  
190 cast state [118]. Instead, a tetragonal Zr<sub>2</sub>Si intermetallic was formed, evenly dispersed, with sizes  
191 ranging from 3 – 10 μm, in the α-Fe matrix, see Figure 10. The compressive yield strength was  
192 measured to be 700 MPa with 13% compression strain to failure at room temperature. Silicon additions  
193 to Ti alloys have been shown to improve creep resistance due to their strong pinning of dislocations,  
194 and grain/lath boundary sliding [166], therefore, further work into the Zr-Si system is warranted.

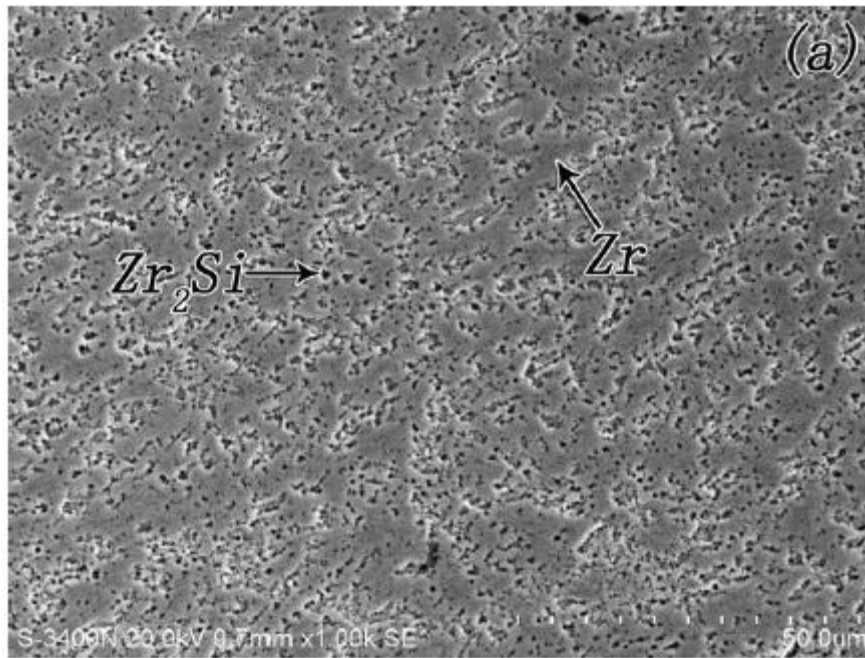


Figure 10. Secondary electron SEM micrograph of as cast Zr-8.8Si. Taken from Ref. [118].

### 3.1.8. Zr-Fe

Iron is a common addition to current Zr alloys due to the strengthening provided by the precipitation of  $ZrFe_2$  (C14) and  $Zr_2Fe$  (C16 Laves phase) secondary phase particles. In the binary system, Fe has a solubility limit of  $\sim 4$  at.%, in  $\alpha$ -Zr, above  $775^\circ\text{C}$ . Below this temperature, Fe is essentially insoluble and will instead form the  $Zr_3Fe$ , an orthorhombic intermetallic, at equilibrium [167]. The diffusion of Fe is relatively fast and segregation to the surface of single crystal samples is observed near instantaneously between temperatures  $450$ - $750^\circ\text{C}$  [168,169].

Dissolution of secondary phase particles is known to occur at high fluence ( $>10^{26}$   $\text{n}\cdot\text{m}^{-2}$ , 20 dpa) due to the effects of displacive radiation. A correlation between an increase in Fe content and  $\langle c \rangle$ -loop dislocation size and density has been made, suggesting that Fe will promote irradiation induced growth [170]. It is unclear as to whether this will translate to fusion environments as thermal creep will likely dominate. However, success in increasing Fe content in conventional Zr alloys (to  $\sim 0.50$  wt.%) has been seen in HiFi<sup>TM</sup> for lowering H pickup in fission environments [171].

### 212 **3.1.9. Zr-Mo**

213 Molybdenum has a large high-temperature solubility in  $\beta$ -Zr ( $\leq 20$  at.% at 1576°C) but is not  
214 soluble below 730°C in  $\alpha$ -Zr. Experimental studies on binary alloys of the two species are typically  
215 made on quenched samples from the  $\beta$ -phase forming region and are considered for room temperature  
216 biomedical applications [120]. At intermediate temperatures (500-730°C) the C15 ZrMo<sub>2</sub> Laves phase  
217 will form [172]. The mechanical properties of two binary mixtures with 0.2 and 1.0 at.% Mo, which  
218 were cold worked, annealed at 750°C for 1 h then annealed at 500-550°C for 3 h, have been measured  
219 at 400°C. It was observed that a linear increase in yield strength from 60 MPa to 130 MPa could be  
220 achieved with increasing Mo content compared to ~20 MPa of the base metal [121]. Hydrogenation  
221 experiments on these samples were also conducted and it was shown that the H retention decreased  
222 with increasing Mo content and when Mo is included at ~1.0 at.% the corrosion resistance of the  
223 material, in water at 350°C, is significantly improved compared to 0.2 and 0.5 at.% mixtures. It is  
224 thought that the ZrMo<sub>2</sub> has a low H absorbency, which is the main contributing factor to the decrease  
225 in H retention. In these samples, it is possible that there is a  $\beta$  phase fraction still present as ageing  
226 studies of Zr alloys containing Mo have shown that complete transformation from  $\beta \rightarrow \alpha$  phase occurs  
227 by 1000 h yet some  $\beta$  phase is still retained after 100 h [173].

### 228 **3.1.10. Zr-V**

229 Vanadium has a small solubility in  $\alpha$ -Zr (1-3 at.% below 863°C) [174]. Above this concentration  
230 the V<sub>2</sub>Zr C15 Laves phase forms [174], and above 863°C a single phase BCC solid solution will form,  
231 which has a solubility of  $\leq 18$  at.%.

232 The mechanical properties of alloys containing 0.2 and 0.5 at.% have been studied previously  
233 [122]. The samples were hot-rolled at 870°C and quenched, and as a result of the quenching, some  $\beta$   
234 phase was retained. Both samples displayed an  $\alpha+\beta$  microstructure and exhibited strengths of 700 MPa  
235 and 820 MPa and elongation of 17% and 20%, respectively. It is expected that the  $\beta$  phase will not  
236 remain, and V<sub>2</sub>Zr precipitation will occur if used in long term operation between 500-700°C.

### 237 **3.1.11. Zr-W**

238 Tungsten has a limited solubility (1-3 at.% below 850°C) in  $\alpha$ -Zr and will form the  $W_2Zr$  C15

239 Laves phase outside these compositional bounds. Above 850°C, W is soluble in  $\beta$ -Zr up to ~5 at.%  
240 [175].

241 A study reporting the mechanical properties of powder processed (34-57 at.% W) samples  
242 reported large compressive strengths at room temperature (1060–2690 MPa) however these samples  
243 were very brittle where fracture at <1.0% tensile strains occurred, attributed to porous defective  
244 structures [123].

### 245 **3.2. Higher order Zr alloys**

246 Higher order advanced Zr based structural alloys with improved room temperature mechanical  
247 properties are a topic of interest in the biomedical community due to their lower magnetic  
248 susceptibility, relative to Ti, and biocompatibility for implants [176]. However, it is the room  
249 temperature mechanical properties of single  $\beta$  phase alloys that are of interest to this community, and  
250 the target for a bulk moduli is 10-30 MPa for their application as implants/prosthetics. Therefore,  
251 ageing studies at intermediate temperatures (500-700°C) are not typically performed and instead  
252 quenching from ~1000°C is routine. Furthermore, the compositions are typically highly alloyed and  
253 present large thermal neutron absorption cross-sections. Nevertheless, the state-of-art pertaining to  
254 each higher order Zr alloy identified for this review is presented in the following subsections. Table 4,  
255 provides a summary of available scientific literature and score calculated identically to the binary  
256 systems. No mechanical property data for >RT were found within this review.

257 **Table 4.** Checklist and tally of the type of data identified within this review to be available within the scientific literature for each higher order Zr system. RT,  $\sigma$  and  $\varepsilon$  refer to  
258 room temperature, stress, and strain, respectively.

Alloy	Microstructure			Mechanical properties	Score	<i>Pros</i>	<i>Cons</i>	Future work
	As-cast	Heat treated 500-700°C	Heat treated >700°C	RT				
				$\sigma$ vs $\epsilon$				
Zr-Ti-Al-(V)	✓ [112-114]	✓ [115-117]	✓ [115-119]	✓ [112,113,115,116,118,119]	4	<ul style="list-style-type: none"> <li>• Good room temperature strength and ductility when furnace cooled.</li> <li>• Can be tailored for <math>\alpha+\beta</math> microstructure at 550-600°C that may provide creep resistance.</li> <li>• The activity of alloying elements within this system are lower than that of pure Zr, ranging from <math>10^7</math>-<math>10^9</math> Bq·kg<sup>-1</sup></li> </ul>	<ul style="list-style-type: none"> <li>• High Ti content will equate to high thermal neutron absorption cross-sections (compositions studied ~2.5 bn).</li> <li>• Faster cooling rates will induce brittle <math>\omega</math> phase formation.</li> <li>• <math>\beta</math>-phase can completely transform to <math>\alpha</math>-phase if ageing occurs past 32 h at 500°C.</li> </ul>	<ul style="list-style-type: none"> <li>• Reduce Ti and V content, to minor alloying additions, to reduce thermal neutron absorption cross-section.</li> <li>• Mechanical property tests should be conducted at elevated temperatures.</li> </ul>
Zr-Al-Sn	✓ [120]		✓ [120]	✓ [120]	3	<ul style="list-style-type: none"> <li>• Low thermal neutron absorption cross-section.</li> <li>• Good as-cast and heat treated mechanical properties at room temperature.</li> </ul>	<ul style="list-style-type: none"> <li>• Potential susceptibility to corrosion in aqueous environments.</li> <li>• Alloying additions of Sn will increase the activity of the alloy.</li> </ul>	<ul style="list-style-type: none"> <li>• Ageing experiments between 500-700°C should be performed to identify Zr-Al precipitate structures and stabilities.</li> <li>• Mechanical properties should be evaluated at RT and elevated temperatures.</li> </ul>
Zr-Mo-Ti	✓ [121]			✓ [121]	2	<ul style="list-style-type: none"> <li>• Has the potential to precipitate harden and solid solution strengthen.</li> <li>• May be more resistant to H absorption.</li> <li>• Good <math>\beta</math>-phase room temperature mechanical properties.</li> </ul>	<ul style="list-style-type: none"> <li>• High thermal neutron absorption cross-section (compositions studied ~1.0 bn).</li> <li>• No microstructural or mechanical property literature exists for temperatures between 500-700°C.</li> <li>• Mo additions will significantly increase the activity.</li> </ul>	<ul style="list-style-type: none"> <li>• Reduction of alloying species and microstructural/mechanical property investigations at temperatures between 500-700°C.</li> </ul>
Zr-Nb-Ti	✓ [122,123]			✓ [122,123]	2	<ul style="list-style-type: none"> <li>• Good room temperature mechanical properties of the <math>\beta</math>-phase.</li> </ul>	<ul style="list-style-type: none"> <li>• High thermal neutron absorption cross-section.</li> <li>• Higher alloying (therefore higher neutron cross-section) is required to stabilise <math>\beta</math>-(Nb,Zr,Ti) phase below 600°C.</li> <li>• Additions of Nb will increase activity of alloy.</li> </ul>	<ul style="list-style-type: none"> <li>• Reduce alloying.</li> <li>• Addition of species to alloy with the BCC Nb phase.</li> </ul>
Zr-Mo-(Sn)			✓ [108]	✓ [108]	2	<ul style="list-style-type: none"> <li>• Relatively good thermal neutron absorption cross-section.</li> <li>• Good room temperature strength with microstructures equilibrated at 500°C.</li> </ul>	<ul style="list-style-type: none"> <li>• Brittle at room temperature.</li> <li>• Mo will significantly increase activity of the alloy.</li> </ul>	<ul style="list-style-type: none"> <li>• Detailed crystallographic and microstructural analyses to determine cause of embrittlement.</li> <li>• Investigate role of cooling rate on microstructure.</li> </ul>

### 3.2.1. Zr-Ti-Al-(V)

Several investigations into the mechanical properties of ternary Zr-Ti-Al alloys have been conducted to-date. However, the focus has been on Ti rich compositions where the alloy with the highest concentration of Zr was 45Ti-40Zr-15Al (at.%). The trend of decreasing  $\alpha \rightarrow \beta$  transition temperature as the ratio between Ti:Zr approaches one, remains true when Al is included in the concentrations studied ( $\leq 15$  at.%) [177]. Conversely, Al additions increase the transition temperature [178]; a concept in agreement with the  $\alpha$ -Ti stabilising effect of Al addition observed in the past. The microstructures of the Zr-Ti-Al alloys are highly dependent on cooling rate and processing conditions and single phase  $\alpha$ ,  $\beta$  or multiphase  $\alpha'$  ( $\beta$  transformed  $\alpha$ ) and  $\alpha''$  (metastable orthorhombic) microstructures have been demonstrated for similar compositions [178,179]. Only the room temperature mechanical properties have been assessed, where UTS ranges from 1000 – 1550 MPa with 3 – 11% uniform elongation.

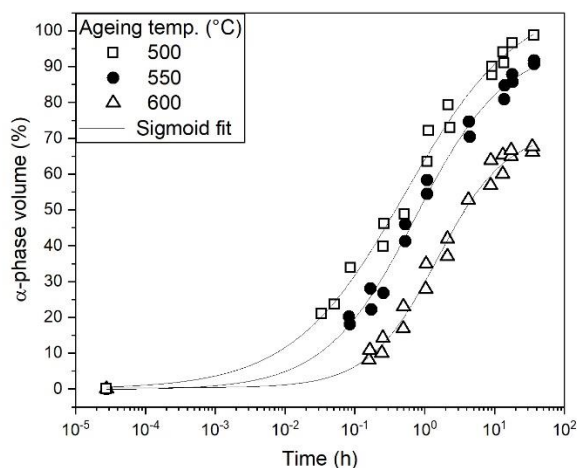
Exploration of the compositions that include V, in the Zr-Ti-Al-V system, originated with Ti-6Al-4V wt.% (Ti-6-4), a dual phase  $\alpha+\beta$  Ti alloy used for aerospace and biomedical applications [180]. In the initial study, 8 – 28 at.% Zr was added to the Ti-6-4 alloy composition [181]. The maximum UTS was measured to be 1317 MPa (increase of 320 MPa compared to Ti-6-4) and elongation of 8% (decrease of 6% compared to Ti-6-4), at room temperature. An additional study reporting the microstructures and mechanical properties of a series of alloys with higher Zr contents (Table 5) within the Zr-Ti-Al-V system was published [182]. These samples were annealed at 850°C for 30 mins, hot rolled, and quenched. Non-equilibrium microstructures of  $\alpha'$  and  $\alpha''$  (metastable orthorhombic) were observed in combination with the  $\beta$  phase for the samples with lowest and second lowest Zr content, respectively. The three Zr richer samples had mixtures of  $\alpha$  and  $\beta$  phase. The room temperature UTS peaked at 1246 MPa for Zr-45Ti-5Al-3V wt.% and stemmed a new branch of research into this composition and its variations where some are referred to as TZAV. The  $\alpha \rightarrow \beta$  transition temperature was investigated in the original study where it was determined that as the Zr content increases, the transition temperature decreases in line with the behaviour of a binary Zr-Ti alloy. Although similar experiments have not been carried out on compositions with  $\gg 50$  at.% Zr, it is expected that the  $\alpha \rightarrow$

287  $\beta$  transition temperature will increase when the Zr:Ti ratio is  $\gg 1$ . However, precipitation of the  $Zr_3Al$   
 288 phase is likely due to the reduced solubility of Al in Zr compared to Ti.

289 Table 5. Example compositions (at.%) of alloys investigated in the Zr-Ti-Al-V system [182].

Zr	Ti	Al	V	UTS (MPa)	Elongation (%)	$\alpha \rightarrow \beta$ transition temperature ( $^{\circ}C$ )
17.3	69.2			1168	3	$\sim 800$
26.0	60.5			1206	10	$\sim 675$
34.5	52.0	$\sim 10.0$	$\sim 3.5$	1246	12	$\sim 625$
43.3	43.2			1040	13	$\sim 575$
51.9	34.6			978	11	$\sim 500$

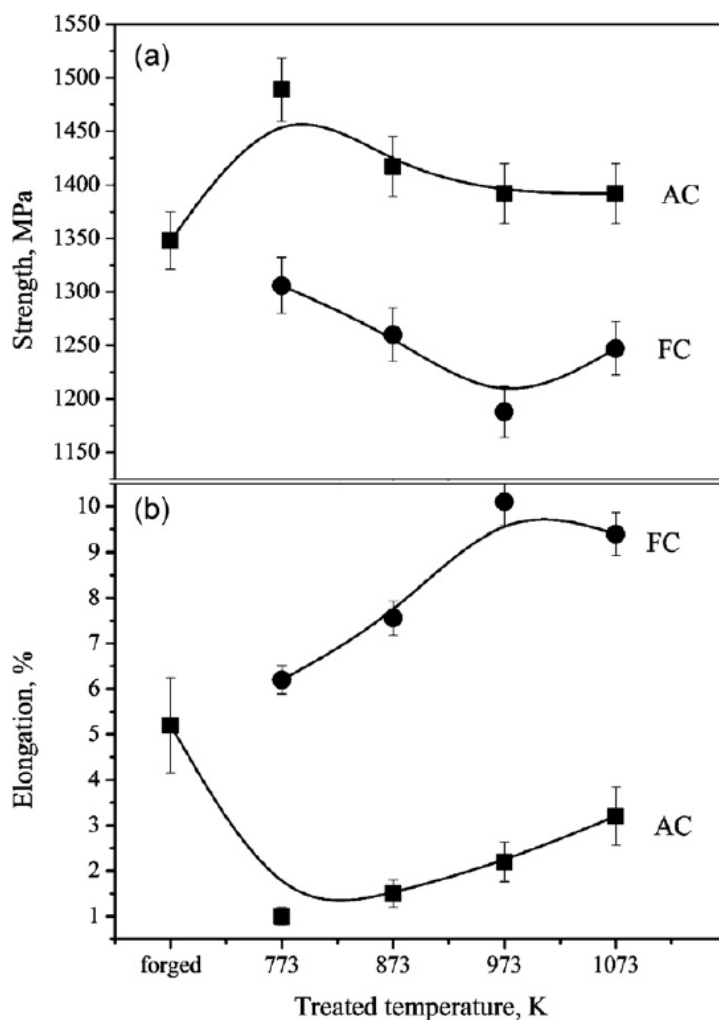
290  
 291 An investigation into the microstructure after ageing at  $500^{\circ}C$ ,  $550^{\circ}C$ , and  $600^{\circ}C$  for 32 h has  
 292 been made on the Zr-45Ti-5Al-3V (wt.%) alloy after solution treatment at  $850^{\circ}C$  and  $1050^{\circ}C$  [183].  
 293 It was determined that regardless of prior solution treatment, the fraction of  $\alpha$ -phase changed  
 294 dramatically within the first 32 h, see Figure 11. As pictured, the  $\beta$ -phase was partially retained in the  
 295  $550^{\circ}C$  aged, and  $600^{\circ}C$  aged samples but 100% of  $\alpha$ -phase was recovered after ageing at  $500^{\circ}C$ . Phase  
 296 changes of this scale, at temperatures relevant to breeder operation, would be undesirable in a structural  
 297 material.



298  
 299 Figure 11. Volume fraction of  $\alpha$ -phase measured by XRD for Zr-45Ti-5Al-3V (wt.%) when aged at  $500^{\circ}C$   
 300 ( $\square$ ),  $550^{\circ}C$  ( $\bullet$ ), and  $600^{\circ}C$  ( $\triangle$ ). Curves fitted using sigmoid functions [183].

301 An additional study on the Zr-45Ti-5Al-3V (wt.%) alloy has been made comparing the  
 302 microstructure and room temperature mechanical properties after annealing samples for 1 h at  $500^{\circ}C$ ,  
 303  $600^{\circ}C$ ,  $700^{\circ}C$ , and  $800^{\circ}C$ , after homogenisation and quench from  $1000^{\circ}C$ . The annealed samples were

304 cooled in air (at a rate of  $10^{\circ}\text{C}\cdot\text{s}^{-1}$ ) and in a furnace ( $0.07^{\circ}\text{C}\cdot\text{s}^{-1}$ ) [184]. It was found that the samples  
 305 that were air cooled to RT from temperatures between 500-800°C had drastically reduced total  
 306 elongations (1-3% from 5.4% in the as-forged state) whereas the samples that were furnace cooled  
 307 increased in ductility, displaying higher total elongations at RT (6-10%), see Figure 12. This was  
 308 attributed to the athermal  $\omega$ -phase formation during the more rapid cooling. These results are also  
 309 supported by a separate study with a similar conclusion on the Zr-40Ti-5Al-4V (wt.%)  
 310 composition [185]. From these results it may be possible to hypothesise that if such cooling rates occur  
 311 in a breeder blanket during pulsed operation the structural material may embrittle significantly.



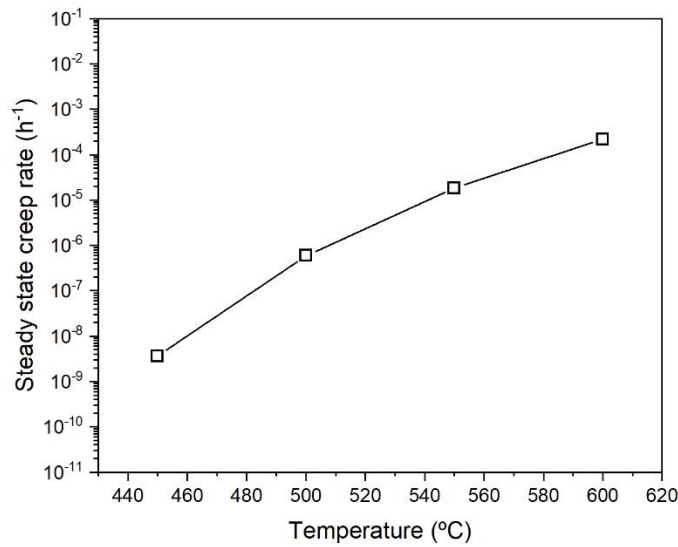
312  
 313 Figure 12. Strength and elongation of Zr-45Ti-5Al-3V (wt.%) after annealing at different temperatures (x-axis)  
 314 for 1 h and air cooling (squares) or furnace cooling (circles) to RT. Taken from Ref [184].

315 Variations of this system have been made with the addition of Fe in concentrations 0.5-2.5  
 316 wt.% [186] and replacement of V with Fe in concentrations of 0.5-2.0 wt.% [187]. However, ageing

317 experiments have not been conducted at 500-700°C and only non-equilibrium microstructures, with  
318 high  $\beta$  phase fractions, quenched from a high temperature  $\geq 850^\circ\text{C}$  have been assessed. It is likely that  
319 at temperatures relevant to a breeder blanket the  $\text{Zr}_3\text{Fe}$  or  $\text{TiFe}$  intermetallic will precipitate due to the  
320 insolubility of Fe in  $\alpha$ -(Zr,Ti). Further work is required to determine the material behaviour at the  
321 relevant temperature range.

322 The thermal creep properties of the Zr-Ti-Al-V system have not been assessed, however, due to  
323 the similarities of Zr and Ti, and substantial amounts of literature on the creep of Ti-6-4 we may draw  
324 some insights into the possible behaviour.

325 The creep process in Ti-6-4 is suggested to be dominated by climb processes of  $\alpha$ -phase  
326 dislocations in the prismatic plane ( $\langle a \rangle$  loops) [188,189]. It should be noted that in Ti alloys, the  $\beta$ -  
327 phase generally exhibits faster diffusion than  $\alpha$  and so the volume fraction of  $\beta$  is often minimised in  
328 high temperature Ti alloys [190]. Nevertheless, dual-phase  $\alpha + \beta$  microstructures are effective in both  
329 Ti and Zr materials for conferring high strength  $\sim 1000$  MPa and good creep resistance  $\sim 400^\circ\text{C}$ .  
330 However, for every  $100^\circ\text{C}$  increase, the creep rate increases by over an order of magnitude, and at  
331  $\sim 525^\circ\text{C}$  the steady-state creep strain rate is  $> 10^{-6} \text{ s}^{-1}$  for applied stresses  $\geq 70$  MPa [189], see Figure 13.  
332 Moreover, the thermal creep rates above  $500^\circ\text{C}$  are likely too high for use of these materials in a  
333 breeder blanket.



334

335 Figure 13. Estimated steady-state creep rate for an applied stress of 70 MPa for Ti-6-4 extrapolated from data  
 336 taken from Ref. [189].

### 337 3.2.2. Zr-Al-Sn

338 One study has been conducted on alloys within the Zr-5Al-(2-6)Sn (wt.%) composition range in  
 339 the context of structural nuclear materials [191]. A single  $\alpha$  phase, lath martensitic structure was  
 340 identified with compressive yield strengths and strains ranging from 835-913 MPa and 18.57-21.43%,  
 341 respectively. Heat treating for 2 h at 900°C and air cooling led to the precipitation of ZrAl  
 342 (orthorhombic), which is likely metastable as one would expect Zr<sub>3</sub>Al from binary phase diagrams.  
 343 Nevertheless, the RT compressive yield strengths were increased to 1003-1044 MPa and the strains  
 344 decreased to 13.03-18.79%.

### 345 3.2.3. Zr-Mo-Ti

346 Alloys within the Zr-Mo-Ti ternary have been investigated by the biomedical research community  
 347 [192]. The compositions Zr-12Mo-(3-11)Ti were quenched from the melt and only single phase  $\beta$   
 348 microstructures were observed. The room temperature yield strengths were found to range from 1200-  
 349 1363 MPa, and the strains to failure ranged from 12-20%, when in compression. However, it is not  
 350 expected that these compositions would retain their single phase  $\beta$  microstructures at operation  
 351 temperatures in a breeder blanket. Instead multiphase microstructure of  $\alpha$ -(Zr,Ti), ZrMo<sub>2</sub> and/or  $\beta$ -  
 352 (Zr,Ti,Mo) is predicted to occur. It is likely that this, along with possible  $\omega$  phase at non-quench  
 353 cooling rates, will contribute greatly to strengthening and the ductility will be reduced further.

### 3.2.4. Zr-Nb-Ti

The compositions that have been investigated to-date are Zr-20Nb-(3-15)Ti [193] and Zr-12Nb-(2-16)Ti [194]. All samples were observed to consist of a single-phase BCC structure except Zr-12Nb-16Ti, which exhibited some  $\omega$ -phase. Relatively good mechanical properties were achieved with strengths ranging from 1000 – 1300 MPa and compressive strains of ~35%.

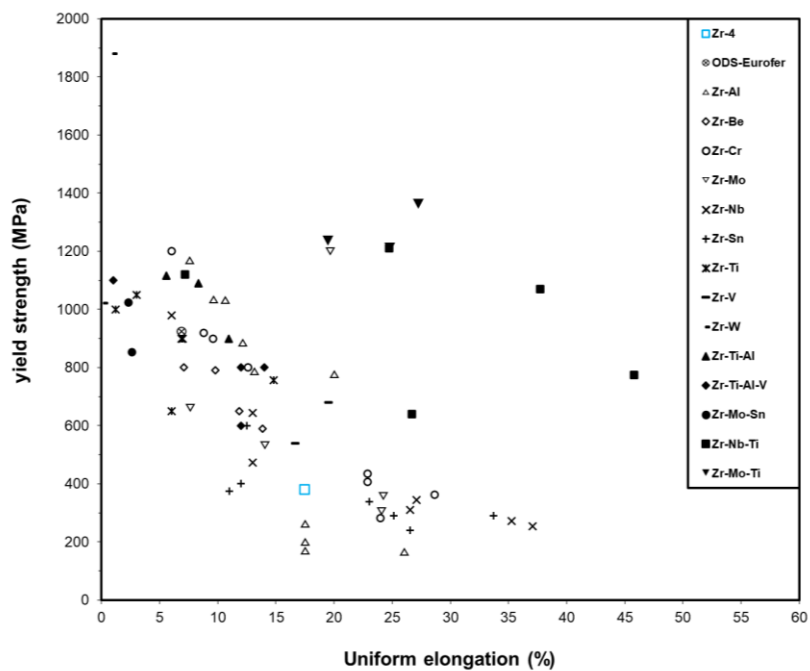
A majority of the lower Ti compositions exist outside the single-phase forming region and will undergo transformations from  $\beta \rightarrow \alpha/\alpha'$  if operated at temperatures ~550°C [157]. However, for higher Nb and Ti contents it may be possible for the single phase  $\beta$  forming region for this ternary system to exist at this temperature.

### 3.2.5. Zr-Mo-(Sn)

Alloys within the Zr-Mo-Sn ternary system were investigated in the 1950-70s in the context of high temperature (500°C) structural materials for fission applications [173]. It was the aim of the investigators to quench the Zr-2.8Mo-1.5Sn (at.%) composition from the  $\alpha + \beta$  (850°C) and  $\beta$  (1000°C) forming regions, anneal at 500°C for 1000 h, and retain a strong high temperature  $\beta$  or transformed ( $\alpha'$ ) phase while maintaining room temperature ductility. The composition tested was Zr-2.8Mo-1.5Sn (at.%). It was reported that for the sample quenched from the  $\beta$  forming region, an  $\alpha + \alpha'$  microstructure was produced, and for the sample quenched from the  $\alpha + \beta$  forming region, an  $\alpha + \alpha' + 10\% \beta$  microstructure was produced. However, the UTS/elongation for each sample were measured to be 853 MPa/2.6% and 1023 MPa/2.3%, respectively, which is too brittle for workability of a structural material. There is insufficient data on the crystallographic analyses of these samples to discount  $\omega$  or intermetallic precipitation, which may have led to the reduction in ductility. Alloys containing Nb and V in 2 at.% contributions were also studied and were found to exhibit lower strengths and lower ductility. It should also be mentioned that Zr-4.7Mo-1.5Sn and Zr-1.8Mo-3.0Sn were investigated, however, were only aged for 8-24 h at 482 - 538°C and therefore likely did not have microstructures or mechanical properties accurately reflecting components in operation at these temperatures.

### 3.3. Comparison of properties

Figure 14 shows the room temperature yield strengths and strains to failure of binary and higher order Zr alloys, experimentally measured in the reviewed studies. There are many systems that present a good combination of room temperature strength and ductility. However, this information is not adequate to provide confidence in their ability to maintain structural integrity at higher temperature operation. Some Zr-Al, Zr-V, Zr-Mo-(Ti) and Zr-Nb-Ti compositions can demonstrate comparable uniform elongations and markedly higher RT strengths than Zr-4. However, the latter three alloy systems present significant BCC phase fractions that are likely unstable at operating temperatures between 500-700°C, and the Zr-Al compositions that can achieve ductile behaviour at RT require a polished surface state.

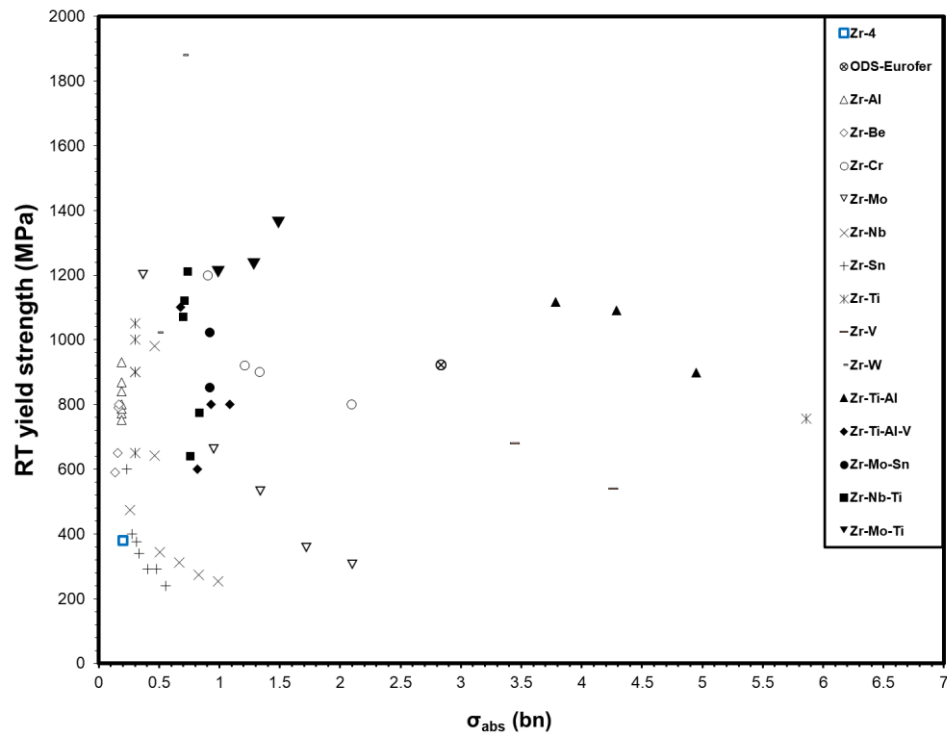


390  
391

392 Figure 14. Room temperature yield strengths of pure Zr, commercial, binary, and higher order Zr alloys and their  
393 tensile strains to failure. The dataset used to construct this figure is accessible from Ref [8].  
394

395 One of the challenges of alloying Zr for nuclear applications is that including most elements in  
396 large quantities (>1 at.%) significantly alters the thermal neutron absorption cross-section ( $\sigma_{\text{abs}}$ ) for  
397 which Zr was selected in the first place. A weighted average of the elemental  $\sigma_{\text{abs}}$  for each Zr alloy was  
398 calculated and plotted against RT yield strength, see Figure 15. It can be seen that binary Zr alloys

399 containing Al, Be, Sn, Ti and Nb present  $\sigma_{\text{abs}}$  values comparable to Zr-4 of 0.2 bn. Zr-Cr, -Mo-Ti, -Nb-  
 400 Ti, -Ti-Al-V display  $\sigma_{\text{abs}}$  values closer to 1.0 bn, which is of similar magnitude to the  ${}^6\text{Li}$  breeding cross-  
 401 section but less than half that of Fe (2.56 bn). Using this method of calculation, the maximum  
 402 concentration of each element allowed before a binary Zr-X alloy exceeds the  $\sigma_{\text{abs}}$  of Zircaloy-4 can be  
 403 estimated, see Table 6. Only Al, Nb and Sn can be alloyed in concentrations  $> 1$  at.%. Be, Mg and Si  
 404 have  $\sigma_{\text{abs}}$  values lower than Zr therefore have no concentration limit.



405  
 406 Figure 15. Room temperature yield strength of experimentally measured alloys plotted against their theoretical  
 407 thermal neutron absorption cross-sections.  
 408

409  
 410  
 411 Table 6. Maximum allowable concentration of element before thermal neutron absorption cross-section exceeds  
 412 that of Zr-4 (0.3 bn) in a binary alloy.

	Al	Be	Cr	Fe	Hf	Mg	Mo	Nb	Ni	Os	Pd
at.%	32.61	-	0.52	0.63	0.01	-	0.65	1.55	0.35	0.09	0.22
	Re	Ru	Sc	Si	Sn	Ta	Ti	V	W	Y	
at.%	0.02	0.63	0.05	-	3.40	0.07	0.25	0.31	0.08	1.37	

413

414

415           When compared to multi-decadal research efforts that have been undertaken for reduced-  
416 activation ferritic/martensitic (RAFM) steels, advanced Zr alloy research is in its infancy. Targeted,  
417 small-scale, laboratory experiments that investigate microstructure and mechanical properties are still  
418 required to make a better judgement as to whether advanced Zr alloys are worth pursuing for use in  
419 operating temperatures between 500-700°C. Castable nano-structured steels currently represent the  
420 state-of-the-art in RAFM steel research and should be used as a mechanical property benchmark for any  
421 future Zr alloys investigated for a similar purpose. A comprehensive overview of the history and current  
422 status of RAFM steels can be found in Ref. [195].

423

### 424           **3.4. High-entropy alloys**

425           High-Entropy Alloys (HEAs), or complex concentrated alloys (CCAs) are alloys consisting of  $\geq 4$   
426 elements in near equiatomic concentrations [196]. This relatively new area of study has seen  
427 tremendous growth over the last 10 years. The original premise of HEAs is that a solid solution phase  
428 is stabilised by the configurational entropy (entropy of mixing), which increases in magnitude with the  
429 addition of more elements, and is maximised when their concentrations are in equal ratio [197,198]. It  
430 is the solid solution phase that is typically the majority phase within a HEA, existing as simple BCC,  
431 FCC or HCP structures. The highly alloyed nature of these phases is thought to contribute greatly to  
432 solid solution strengthening and allow for higher strengths than conventional alloys while maintaining  
433 ductility [199].

434           Difficulties arise in maintaining the solid solution phase when ageing at temperatures between  
435 400-1000°C. This is because the entropy term is a prefactor to temperature in the equation for Gibbs  
436 free energy, and typically stabilises the solid solution phase at temperatures close to melting.  
437 Therefore, for lower temperatures more commensurate with that of breeder blanket operation in a  
438 fusion reactor, decomposition of the solid solution phase and precipitation of intermetallics is more  
439 likely, and is observed to occur in many ageing/annealing experiments for HEAs [200–203]. Whilst  
440 assessments of the room temperature properties of as-cast/solution treated and quenched HEAs is  
441 commonly performed, a significantly smaller fraction of thermal ageing studies have been performed  
442 on HEAs, and fewer still assess mechanical properties of equilibrium microstructures at elevated

443 temperatures [204]. Nevertheless, very high strengths (~2.3 GPa) have been observed in BCC HEAs  
444 that also show a higher resistance to softening than Ni superalloys at elevated temperatures (500 –  
445 1000°C) [204,205]. Further, some HEAs are reported to have good tolerance to irradiation damage  
446 [206,207].

447 In the context of Zr alloys for fusion, by definition a HEA cannot contain a majority portion of  
448 Zr in the mixture and therefore the  $\sigma_{\text{abs}}$  will largely depend on the other elements in the alloy. The Nb-  
449 Ti-V-Zr system has been identified as one of the single phase HEA systems with the lowest  $\sigma_{\text{abs}}$ , which  
450 is still on the order of steels [208]. It may be possible that the increased strength of such alloys is  
451 sufficiently high that a reduced amount of structural fraction can be used and therefore less absorption  
452 of neutrons compared to other candidate materials. However, if a very low  $\sigma_{\text{abs}}$  ( $\leq 0.2$  bn) HEA is  
453 desired it would be based upon the low  $\sigma_{\text{abs}}$ , elements Al, Be, Mg, Pb, and Si, with Zr, where a single-  
454 phase solid solution is unlikely to be achievable due to the largely favourable formation energies for  
455 intermetallic compounds. The binary mixtures alone present many different possible intermetallic  
456 phases, which among them are some ordered HCP structures, e.g.,  $\text{Zr}_3\text{Al}$ ,  $\text{Be}_2\text{Zr}$ ,  $\text{Zr}_5\text{Pb}_3$ , that may  
457 maintain some measure of ductility. However, the low melting temperatures of Al, Mg, and Pb are a  
458 concern. Nevertheless, opportunities still may exist in multi-phase low  $\sigma_{\text{abs}}$  HEAs.

459 *Pros:* BCC refractory metal HEAs can exhibit high strengths and resistance to softening at higher  
460 temperatures, and further, some HEAs may be resistant to irradiation damage.

461 *Cons:* Zr will not contribute a majority concentration to the alloy and therefore the thermal neutron  
462 absorption cross-section will rely on the other alloying species, this leads to previously studied HEAs,  
463 which have cross-sections comparable to steel. Therefore, the alloying species are restricted to Al, Be,  
464 Mg, Pb, and Si if a maintenance of  $\leq 0.2$  bn is desired, however, these are likely to be low melting  
465 temperatures multiphase, and brittle.

466 Future work: Investigations into multiphase, low  $\sigma_{\text{abs}}$  (0.2 bn) HEAs formed between Zr, Al, Be,  
467 Mg, Pb, and Si species or very high strength, moderate  $\sigma_{\text{abs}}$  (2.0 bn) HEAs should be made and their  
468 microstructures and mechanical properties assessed from RT to 700°C.

#### 4. Summary and Conclusions

Zirconium alloys have seen prevalent use in the nuclear industry for power generation by fission.

This is largely due to its low thermal neutron absorption cross-section ( $\sigma_{\text{abs}}$ ). Past publications have alluded to the utility of Zr alloys in a fusion reactor [1,23]. Indeed, the utilisation of Zr alloys would be of great benefit due to their current production in tonnage quantities with a very well established industry that works to nuclear standards with associated well developed machining, inspection techniques, and knowledge base. Thus enabling rapid screening of current commercial Zr alloys for fusion.

Here, we predict that by using Zr-4 as a structural material in the breeder blanket, the tritium breeding ratio (TBR) is markedly improved over other candidate materials (EUROFER 97, V-4Cr-4Ti, SiC/SiC) for structural fractions  $\leq 0.8$ . However, current commercial Zr alloys do not have adequate strength, creep resistance, and fatigue properties at the temperatures of 500-700°C, at which some blanket designs in DEMO-like fusion reactors are expected to operate [5,9]. Further, embrittlement due to impurity elements such as H, He and corrosion from the coolant will likely occur and barrier coatings between the structural alloy/plasma, /breeder and /coolant will need to be employed. For these reasons, the use of Zr alloys may be more suited to a water-cooled lithium lead (WCLL) breeder blanket concept, which operates in the temperature range 280 – 325 °C and nominal for fission reactors. However, this review was conducted to explore the landscape and potential novel Zr alloys that can achieve adequate mechanical properties at temperatures, above nominal for fission reactors, between 500-700°C.

Initial screening of the mechanical properties and thermal neutron absorption cross-sections of advanced Zr alloys has identified systems that have demonstrated adequate room temperature properties. Of these systems, Zr-Al has been studied the most extensively for its potential use as a  $\text{Zr}_3\text{Al}$  structural intermetallic cladding material in fission applications. Some compositions have been reported to achieve room temperature ductility ( $\geq 5\%$  uniform elongation), high strengths ( $\geq 800$  MPa), resistance to high temperature softening, and good creep resistance. However, ductility issues arise in unpolished components, and poor corrosion resistance is noted in aqueous environments. Any additional development of these alloys should be done through alloying of other species, in an attempt to address these shortcomings.

496 The alloying of Sn and Zr is historically an attractive method of increasing creep resistance in  
497 conventional Zr alloys while maintaining a low thermal neutron cross-section. However, in the binary  
498 form it offers inadequate strengthening. There is potential for future work in the Zr-Al-Sn system as it  
499 has a very low thermal neutron absorption cross-section and is strengthened by solid solution and  
500 precipitation while maintaining a ductile nature at room temperature. However, such a system is likely  
501 to be susceptible to aqueous corrosion and is better suited to breeder blankets with non-aqueous cooling  
502 systems. The mixture of Nb and/or O in Zr alloys may provide an option for resistance to aqueous  
503 corrosion and H pickup.

504 A common theme among the studies to-date is that microstructural and mechanical property data  
505 pertaining to samples aged at temperatures relevant to a breeder blanket (500-700°C) is lacking. Instead,  
506 the majority of studies quench from the annealed condition in the  $\beta$ -phase forming region (800-1000°C).  
507 Long term operation at temperatures below the  $\beta$ -phase solvus will decompose the  $\beta$ -phase and therefore  
508 these studies are not a good indicator of material performance at the proposed temperatures.

509 To preserve the low  $\sigma_{\text{abs}}$  that Zr alloys are known for, only Al, Be, Nb, Si, Sn and Y can be alloyed  
510 in concentrations >1 at.%. Equilibrium microstructures are important to characterise at temperatures  
511 between 500-700°C due to kinetics being sufficient for equilibrium to be achieved. Therefore,  
512 precipitate structures, morphologies and their influence on mechanical properties must also be  
513 characterised. When an alloy is identified that can maintain adequate strength ( $\geq 400$  MPa) at this  
514 temperature range, tertiary screening, i.e. creep, irradiation testing, corrosion from aqueous and liquid  
515 metals (Li/Pb) and H/He embrittlement, should be conducted. It is recommended that higher order Zr  
516 alloys combining the aforementioned low  $\sigma_{\text{abs}}$  elements are explored, especially as Be has been shown  
517 to strengthen but not embrittle and increase corrosion resistance and Si has potential to do the same.

518 In terms of nuclear waste production, Zr alloys are predicted to decay cool to an activity of  $\sim 10^8$   
519 (Bq·kg<sup>-1</sup>) after 100 years post-service, nearly an order of magnitude larger than EUROFER 97, where  
520 both fail to meet the UK fusion low level waste limit. We suggest that it may not be practicable to  
521 produce a Zr based component that both meets the proposed mechanical and waste requirements for a

522 breeder blanket. Further, some of the recommended low thermal absorption neutron cross-section  
523 elements (Be, Nb, and Sn) will increase the activity of such components. Therefore, an approach of “as  
524 low as reasonably practicable” may be more suitable in order to harness the neutron efficiency advantage  
525 of Zr for tritium breeding. Further cost-benefit analysis is required in this area.

## 526 **5. Acknowledgements**

527 The Authors would like to acknowledge funding from EPSRC (EP/T012250/1) and  
528 (EP/S01702X/1) for time and resources. As well as Profs. Ted Derby, Michael Preuss, Erland Schulson,  
529 and Steven Zinkle for discussion regarding subject matter of this review.

530 A Knowles acknowledges UKRI Future Leaders Fellowship, Royal Academy of Engineering  
531 Research Fellowship, EUROfusion Research Grant and EPSRC (EP/T01220X/1).

532 Acknowledgement to authors of internal reports, used to guide the writing of this review, should  
533 also be given. These people include: F. Barton, J Bernard, F. Lowrie, C. Riley and M. Rogers from  
534 Rolls-Royce plc, and P. Binks, S. Foster and M. Green from the John Wood Group plc.

535

## 536 **6. References**

537

- 538 [1] T.R. Barrett, G. Ellwood, G. Pérez, M. Kovari, M. Fursdon, F. Domptail, S. Kirk, S.C. McIntosh, S.  
539 Roberts, S. Zheng, Progress in the engineering design and assessment of the European DEMO first wall  
540 and divertor plasma facing components, *Fusion Eng. Des.* 109 (2016) 917–924.
- 541 [2] M. Sandzelius, Fusion potential for spherical and compact tokamaks, (2003).
- 542 [3] A. Sykes, A.E. Costley, C.G. Windsor, O. Asunta, G. Brittles, P. Buxton, V. Chuyanov, J.W. Connor,  
543 M.P. Gryaznevich, B. Huang, Compact fusion energy based on the spherical tokamak, *Nucl. Fusion.* 58  
544 (2017) 16039.
- 545 [4] P.-H. Rebut, ITER: the first experimental fusion reactor, *Fusion Eng. Des.* 30 (1995) 85–118.
- 546 [5] G. Federici, R. Kemp, D. Ward, C. Bachmann, T. Franke, S. Gonzalez, C. Lowry, M. Gadomska, J.  
547 Harman, B. Meszaros, Overview of EU DEMO design and R&D activities, *Fusion Eng. Des.* 89 (2014)  
548 882–889.
- 549 [6] E. Gibney, UK hatches plan to build world’s first fusion power plant., *Nature.* (2019).
- 550 [7] Z. Shanliang, W. Yican, Neutronic comparison of tritium-breeding performance of candidate tritium-  
551 breeding materials, *Plasma Sci. Technol.* 5 (2003) 1995.
- 552 [8] D.J.M. King, High Temperature Zirconium Alloys for Fusion Energy dataset, (2020).  
553 <https://doi.org/http://dx.doi.org/10.17632/c7fy75wrhr.1>.
- 554 [9] T. Ihli, T.K. Basu, L.M. Giancarli, S. Konishi, S. Malang, F. Najmabadi, S. Nishio, A.R. Raffray, C.V.S.  
555 Rao, A. Sagara, Review of blanket designs for advanced fusion reactors, *Fusion Eng. Des.* 83 (2008)  
556 912–919.
- 557 [10] M. Nakamura, K. Tobita, Y. Someya, H. Tanigawa, W. Gulden, Y. Sakamoto, T. Araki, K. Watanabe,  
558 H. Matsumiya, K. Ishii, Key aspects of the safety study of a water-cooled fusion DEMO reactor, *Plasma*  
559 *Fusion Res.* 9 (2014) 1405139.
- 560 [11] M.R. Gilbert, S. Zheng, R. Kemp, L.W. Packer, S.L. Dudarev, J.-C. Sublet, Comparative assessment of  
561 material performance in demo fusion reactors, *Fusion Sci. Technol.* 66 (2014) 9–17.
- 562 [12] K. Ehrlich, The development of structural materials for fusion reactors, *Philos. Trans. R. Soc. London.*  
563 *Ser. A Math. Phys. Eng. Sci.* 357 (1999) 595–623.
- 564 [13] L.M. Giancarli, M.-Y. Ahn, I. Bonnett, C. Boyer, P. Chaudhuri, W. Davis, G. Dell’Orco, M. Iseli, R.  
565 Michling, J.-C. Nevriere, ITER TBM Program and associated system engineering, *Fusion Eng. Des.* 136  
566 (2018) 815–821.
- 567 [14] L.M. Giancarli, X. Bravo, S. Cho, M. Ferrari, T. Hayashi, B.-Y. Kim, A. Leal-Pereira, J.-P. Martins, M.  
568 Merola, R. Pascal, Overview of recent ITER TBM Program activities, *Fusion Eng. Des.* 158 (2020)  
569 111674.
- 570 [15] I. Ricipito, F. Cismondi, G. Federici, Y. Poitevin, M. Zmitko, European TBM programme: First  
571 elements of RoX and technical performance assessment for DEMO breeding blankets, *Fusion Eng. Des.*  
572 156 (2020) 111584.

- 573 [16] S. Kass, The development of the zircalloys, in: Corros. Zircon. Alloy., ASTM International, 1964.
- 574 [17] D.O. Northwood, Irradiation damage in zirconium and its alloys, *At. Energy Rev.* 15 (1977) 547–610.
- 575 [18] D.O. Northwood, R.W. Gilbert, L.E. Bahen, P.M. Kelly, R.G. Blake, A. Jostsons, P.K. Madden, D.
- 576 Faulkner, W. Bell, R.B. Adamson, Characterization of neutron irradiation damage in zirconium alloys—
- 577 an international “round-robin” experiment, *J. Nucl. Mater.* 79 (1979) 379–394.
- 578 [19] A. Rogerson, Irradiation growth in zirconium and its alloys, *J. Nucl. Mater.* 159 (1988) 43–61.
- 579 [20] D. Kaddour, S. Frechinet, A.-F. Gourgues, J.-C. Brachet, L. Portier, A. Pineau, Experimental
- 580 determination of creep properties of zirconium alloys together with phase transformation, *Scr. Mater.* 51
- 581 (2004) 515–519.
- 582 [21] C.B.A. Forty, P.J. Karditsas, The potential use of zirconium-based alloys in fusion power plants, in: 17th
- 583 IEEE/NPSS Symp. Fusion Eng. (Cat. No. 97CH36131), IEEE, 1997: pp. 849–852.
- 584 [22] A. Billerey, Evolution of fuel rod support under irradiation—Impact on the mechanical behaviour of fuel
- 585 assemblies, *Struct. Behav. Fuel Assem. Water Cool. React.* (2005) 101–111.
- 586 [23] C.B.A. Forty, P.J. Karditsas, Uses of zirconium alloys in fusion applications, *J. Nucl. Mater.* 283 (2000)
- 587 607–610.
- 588 [24] Y. Xiao, A. V Sandwijk, Y. Yang, V. Laging, New routes for the production of reactor grade zirconium,
- 589 *Molten Salts Chem. Technol.* (2014) 389–401.
- 590 [25] K.J. Schulz, J.H. DeYoung, R.R. Seal, D.C. Bradley, Zirconium and Hafnium, in: *Crit. Miner. Resour.*
- 591 *United States Econ. Environ. Geol. Prospect. Futur. Supply*, Geological Survey, 2018: pp. V3–V26.
- 592 [26] H.G. Rickover, L.D. Geiger, B. Lustman, History of the development of zirconium alloys for use in
- 593 nuclear reactors, Energy Research and Development Administration, Washington, DC (USA). Div ...,
- 594 1975.
- 595 [27] ATI, Allegheny Technologies Incorporated, Reactor Grade Zirconium, Pittsburgh, 2015.
- 596 [28] J.L. Vandegrift, P.M. Price, J.-P. Stroud, C.J. Parga, I.J. Van Rooyen, B.J. Jaques, D.P. Butt, Oxidation
- 597 behavior of Zirconium, Zircaloy-3, Zircaloy-4, Zr-1Nb, and Zr-2.5 Nb in air and oxygen, *Nucl. Mater.*
- 598 *Energy.* 20 (2019) 100692.
- 599 [29] D.A. Blokhin, V.M. Chernov, A.I. Blokhin, N.A. Demin, I. V Sipachev, Nuclear physical properties of
- 600 zirconium alloys E110 and E635 under long-term neutron irradiation in VVER-1000 reactor, *Inorg.*
- 601 *Mater. Appl. Res.* 3 (2012) 124–128.
- 602 [30] C.M. Eucken, P.T. Finden, S. Trapp-Pritsching, H.G. Weidinger, Influence of chemical composition on
- 603 uniform corrosion of zirconium-base alloys in autoclave tests, in: *Zircon. Nucl. Ind. Eighth Int. Symp.*,
- 604 ASTM International, 1989.
- 605 [31] L. Lunde, R.C. Asher, G. Slattery, F.W. Trowse, C. Tyzack, E. Tolksdorf, Zirconium alloys, (1980).
- 606 [32] M. Steinbrück, M. Böttcher, Air oxidation of Zircaloy-4, M5® and ZIRLO™ cladding alloys at high
- 607 temperatures, *J. Nucl. Mater.* 414 (2011) 276–285.
- 608 [33] S. Yagnik, A. Garde, Zirconium Alloys for LWR Fuel Cladding and Core Internals, *Struct. Alloy. Nucl.*
- 609 *Energy Appl.* (2019) 247–291.
- 610 [34] L.A. Simpson, C.K. Chow, Effect of metallurgical variables and temperature on the fracture toughness of
- 611 zirconium alloy pressure tubes, in: *Zircon. Nucl. Ind.*, ASTM International, 1987.
- 612 [35] P.H. Davies, C.P. Stearns, Fracture toughness testing of Zircaloy-2 pressure tube material with radial
- 613 hydrides using direct-current potential drop, in: *Fract. Mech. Seventeenth Vol.*, ASTM International,
- 614 1986.
- 615 [36] A.T. Motta, L. Capolungo, L.-Q. Chen, M.N. Cinbiz, M.R. Daymond, D.A. Koss, E. Lacroix, G. Pastore,
- 616 P.-C.A. Simon, M.R. Tonks, Hydrogen in zirconium alloys: A review, *J. Nucl. Mater.* 518 (2019) 440–
- 617 460.
- 618 [37] V.M. Chernov, B.K. Kardashev, K.A. Moroz, Low-temperature embrittlement and fracture of metals
- 619 with different crystal lattices—Dislocation mechanisms, *Nucl. Mater. Energy.* 9 (2016) 496–501.
- 620 [38] R. Liu, W. Zhou, J. Cai, Multiphysics modeling of accident tolerant fuel-cladding U3Si2-FeCrAl
- 621 performance in a light water reactor, *Nucl. Eng. Des.* 330 (2018) 106–116.
- 622 [39] J. Cheng, Y. Wu, W. Tian, G. Su, S. Qiu, Neutronics and thermo-hydraulic design of supercritical-water
- 623 cooled solid breeder TBM, *Fusion Eng. Des.* 92 (2015) 52–58.
- 624 [40] IAEA-TECDOC-1496, Thermophysical Properties Database of Materials for Light Water Reactors and
- 625 Heavy Water Reactors, (2006).
- 626 [41] B.A. Cheadle, The physical metallurgy of zirconium alloys, Atomic Energy of Canada Limited, 1975.
- 627 [42] R.E. Macherey, C.H. Bean, N.J. Carson Jr, J.R. Lindgren, Manufacture of Fuel Plates for the
- 628 Experimental Boiling Water Reactor, Argonne National Lab., Lemont, Ill., 1957.
- 629 [43] R. Li, P. Zhang, X. Li, C. Zhang, J. Zhao, First-principles study of the behavior of O, N and C impurities
- 630 in vanadium solids, *J. Nucl. Mater.* 435 (2013) 71–76.
- 631 [44] D.R. Diercks, B.A. Loomis, Alloying and impurity effects in vanadium-base alloys, *J. Nucl. Mater.* 141
- 632 (1986) 1117–1124.

- 633 [45] M.L. Grossbeck, J.F. King, D.J. Alexander, P.M. Rice, G.M. Goodwin, Development of techniques for  
634 welding V–Cr–Ti alloys, *J. Nucl. Mater.* 258 (1998) 1369–1374.
- 635 [46] R.J. Kurtz, K. Abe, V.M. Chernov, V.A. Kazakov, G.E. Lucas, H. Matsui, T. Muroga, G.R. Odette, D.L.  
636 Smith, S.J. Zinkle, Critical issues and current status of vanadium alloys for fusion energy applications, *J.*  
637 *Nucl. Mater.* 283 (2000) 70–78.
- 638 [47] A.M. Garde, H.M. Chung, T.F. Kassner, Uniaxial tensile properties of Zircaloy containing oxygen:  
639 summary report, Argonne National Lab., Ill.(USA), 1977.
- 640 [48] J.R. Theaker, R. Choubey, G.D. Moan, S.A. Aldridge, L. Davis, R.A. Graham, C.E. Coleman,  
641 Fabrication of Zr-2.5 Nb pressure tubes to minimize the harmful effects of trace elements, in: *Zircon.*  
642 *Nucl. Ind. Tenth Int. Symp.*, ASTM International, 1994.
- 643 [49] G. Vigna, L. Lanzani, G. Domizzi, S.E. Bermudez, J. Ovejero-García, R. Piotrkowski, Effect of carbides  
644 on the hydriding and oxidation behavior of a Zr-2.5 Nb alloy, *J. Nucl. Mater.* 218 (1995) 18–29.
- 645 [50] R.A. Ploc, Residual carbon impurities in Zr–2.5 Nb and their effect on deuterium pickup, *J. Nucl. Mater.*  
646 279 (2000) 344–350.
- 647 [51] M.R. Gilbert, T. Eade, T. Rey, R. Vale, C. Bachmann, U. Fischer, N.P. Taylor, Waste implications from  
648 minor impurities in European DEMO materials, *Nucl. Fusion.* 59 (2019) 76015.
- 649 [52] C.E. Eells, Hydride precipitates in zirconium alloys (A review), *J. Nucl. Mater.* 28 (1968) 129–151.
- 650 [53] S. Suman, M.K. Khan, M. Pathak, R.N. Singh, J.K. Chakravarty, Hydrogen in Zircaloy: Mechanism and  
651 its impacts, *Int. J. Hydrogen Energy.* 40 (2015) 5976–5994.
- 652 [54] J.W. Davis, M.A. Ulrickson, R.A. Causey, Use of titanium in fusion components, *J. Nucl. Mater.* 212  
653 (1994) 813–817.
- 654 [55] P.L. Andrew, M.A. Pick, Review of tritium retention in first-wall materials, *J. Nucl. Mater.* 212 (1994)  
655 111–117.
- 656 [56] M.A. Tunes, R.W. Harrison, G. Greaves, J.A. Hinks, S.E. Donnelly, Effect of He implantation on the  
657 microstructure of zircaloy-4 studied using in situ TEM, *J. Nucl. Mater.* 493 (2017) 230–238.
- 658 [57] M.R. Gilbert, S.L. Dudarev, S. Zheng, L.W. Packer, J.-C. Sublet, An integrated model for materials in a  
659 fusion power plant: transmutation, gas production, and helium embrittlement under neutron irradiation,  
660 *Nucl. Fusion.* 52 (2012) 83019.
- 661 [58] M. Steinbrueck, F.O. da Silva, M. Grosse, Oxidation of Zircaloy-4 in steam-nitrogen mixtures at 600–  
662 1200° C, *J. Nucl. Mater.* 490 (2017) 226–237.
- 663 [59] I. Bepalov, M. Datler, S. Buhr, W. Drachsel, G. Rupprechter, Y. Suchorski, Initial stages of oxide  
664 formation on the Zr surface at low oxygen pressure: An in situ FIM and XPS study, *Ultramicroscopy.*  
665 159 (2015) 147–151.
- 666 [60] T. Ahmed, L.H. Keys, The breakaway oxidation of zirconium and its alloys a review, *J. Less Common*  
667 *Met.* 39 (1975) 99–107.
- 668 [61] B. Cox, Oxidation of Zirconium and its Alloys, in: *Adv. Corros. Sci. Technol.*, Springer, 1976: pp. 173–  
669 391.
- 670 [62] F.J.E.J.S. Leistikow, Zircaloy Fuel Cladding Behavior in a LOCA -A Review, in: *Zircon. Nucl. Ind.*  
671 *Seventh Int. Symp.*, ASTM International, 1985: pp. 24–27.
- 672 [63] A.T. Motta, A. Couet, R.J. Comstock, Corrosion of zirconium alloys used for nuclear fuel cladding,  
673 *Annu. Rev. Mater. Res.* 45 (2015) 311–343.
- 674 [64] S. Xie, B. Zhou, X. Liang, Q. Li, W. Liu, M. Yao, J. Zhang, The Distribution of Li Ions in the Oxide  
675 Film Formed on Zircaloy-4 Corroded in Lithiated Water at 633 K, *Materials (Basel).* 13 (2020) 873.
- 676 [65] C.W. Bale, The Li– Zr (Lithium-Zirconium) system, *Bull. Alloy Phase Diagrams.* 8 (1987) 48–50.
- 677 [66] M.G. Nicholas, C.F. Old, Liquid metal embrittlement, *J. Mater. Sci.* 14 (1979) 1–18.
- 678 [67] B. Cox, Y.-M. Wong, Liquid metal embrittlement of Zr-2.5% Nb alloy, *J. Nucl. Mater.* 245 (1997) 34–  
679 43.
- 680 [68] R.F. Koenig, W.A. Heywood, Corrosion of Zirconium and Its Alloys in Liquid Metals, Knolls Atomic  
681 Power Laboratory, 1953.
- 682 [69] J. Zhang, P. Hosemann, S. Maloy, Models of liquid metal corrosion, *J. Nucl. Mater.* 404 (2010) 82–96.
- 683 [70] K.A. Terrani, Accident tolerant fuel cladding development: Promise, status, and challenges, *J. Nucl.*  
684 *Mater.* 501 (2018) 13–30.
- 685 [71] J.-C. Brachet, I. Idarraga-Trujillo, M. Le Flem, M. Le Saux, V. Vandenberghe, S. Urvoy, E. Rouesne, T.  
686 Guilbert, C. Toffolon-Masclat, M. Tupin, Early studies on Cr-Coated Zircaloy-4 as enhanced accident  
687 tolerant nuclear fuel claddings for light water reactors, *J. Nucl. Mater.* 517 (2019) 268–285.
- 688 [72] L.-M. Luo, Y.-L. Liu, D.-G. Liu, L. Zheng, Y.-C. Wu, Preparation technologies and performance studies  
689 of tritium permeation barriers for future nuclear fusion reactors, *Surf. Coatings Technol.* (2020) 126301.
- 690 [73] A. Jain, S.P. Ong, G. Hautier, W. Chen, W.D. Richards, S. Dacek, S. Cholia, D. Gunter, D. Skinner, G.  
691 Ceder, Commentary: The Materials Project: A materials genome approach to accelerating materials  
692 innovation, *Apl Mater.* 1 (2013) 11002.

- 693 [74] R. Gauntt, D. Kalinich, J. Cardoni, J. Phillips, A. Goldmann, S. Pickering, M. Francis, K. Robb, L. Ott,  
694 D. Wang, Fukushima Daiichi accident study (status as of April 2012), Sandia Rep. Sand. 6173 (2012).
- 695 [75] M. Kuznetsov, J. Grune, A. Friedrich, K. Sempert, W. Breitung, T. Jordan, Hydrogen-air deflagrations  
696 and detonations in a semi-confined flat layer, in: Fire Explos. Hazards, Proc. Sixth Int. Semin. (Edited by  
697 D. Bradley, G. Makhviladze V. Molkov), 2011: pp. 125–136.
- 698 [76] L. Baker Jr, Hydrogen-generating reactions in LWR severe accidents, Argonne National Lab., 1983.
- 699 [77] J. Yanez, M. Kuznetsov, A. Souto-Iglesias, An analysis of the hydrogen explosion in the Fukushima-  
700 Daiichi accident, *Int. J. Hydrogen Energy*. 40 (2015) 8261–8280.
- 701 [78] B. Kolbasov, C. Barnes, J. Blevins, ITER plant systems, (1991).
- 702 [79] B.R. Sehgal, Nuclear safety in light water reactors: severe accident phenomenology, Academic Press,  
703 2011.
- 704 [80] M. Lukacs, L.G. Williams, Nuclear safety issues for fusion power plants, *Fusion Eng. Des.* 150 (2020)  
705 111377.
- 706 [81] D. Maisonnier, I. Cook, P. Sardain, R. Andreani, L. Di Pace, R. Forrest, L. Giancarli, S. Hermsmeyer, P.  
707 Norajitra, N. Taylor, A conceptual study of commercial fusion power plants. Final Report of the  
708 European Fusion Power Plant Conceptual Study (PPCS), EFDA Rep. Number EFDA (05)-27/4.10.  
709 (2005).
- 710 [82] M.E. Sawan, M.A. Abdou, Physics and technology conditions for attaining tritium self-sufficiency for  
711 the DT fuel cycle, *Fusion Eng. Des.* 81 (2006) 1131–1144.
- 712 [83] P.K. Romano, N.E. Horelik, B.R. Herman, A.G. Nelson, B. Forget, K. Smith, OpenMC: A state-of-the-  
713 art Monte Carlo code for research and development, in: SNA+ MC 2013-Joint Int. Conf. Supercomput.  
714 Nucl. Appl. Monte Carlo, EDP Sciences, 2014: p. 6016.
- 715 [84] T. Eade, M. Garcia, R. Garcia, F. Ogando, P. Pereslavitsev, J. Sanz, G. Stankunas, A. Travleev,  
716 Activation and decay heat analysis of the European DEMO blanket concepts, *Fusion Eng. Des.* 124  
717 (2017) 1241–1245.
- 718 [85] F. Moro, A. Del Nevo, D. Flammini, E. Martelli, R. Mozzillo, S. Noce, R. Villari, Neutronic analyses in  
719 support of the WCLL DEMO design development, *Fusion Eng. Des.* 136 (2018) 1260–1264.
- 720 [86] L.A. El-Guebaly, A. Team, ARIES-ST nuclear analysis and shield design, *Fusion Eng. Des.* 65 (2003)  
721 263–284.
- 722 [87] L. El-Guebaly, L. Mynsberge, A. Davis, C. D’Angelo, A. Rowcliffe, B. Pint, A.-A. Team, Design and  
723 evaluation of nuclear system for ARIES-ACT2 power plant with DCLL blanket, *Fusion Sci. Technol.* 72  
724 (2017) 17–40.
- 725 [88] M.R. Gilbert, M. Fleming, J.-C. Sublet, Automated inventory and material science scoping calculations  
726 under fission and fusion conditions, *Nucl. Eng. Technol.* 49 (2017) 1346–1353.
- 727 [89] I. Cook, D. Maisonnier, N.P. Taylor, D.J. Ward, P. Sardain, L. Di Pace, L. Giancarli, S. Hermsmeyer, P.  
728 Norajitra, R. Forrest, European fusion power plant studies, *Fusion Sci. Technol.* 47 (2005) 384–392.
- 729 [90] M.R. Gilbert, T. Eade, C. Bachmann, U. Fischer, N.P. Taylor, Activation, decay heat, and waste  
730 classification studies of the European DEMO concept, *Nucl. Fusion*. 57 (2017) 46015.
- 731 [91] R.E. Melchers, On the ALARP approach to risk management, *Reliab. Eng. Syst. Saf.* 71 (2001) 201–  
732 208.
- 733 [92] L. V Boccaccini, G. Aiello, J. Aubert, C. Bachmann, T. Barrett, A. Del Nevo, D. Demange, L. Forest, F.  
734 Hernandez, P. Norajitra, Objectives and status of EUROfusion DEMO blanket studies, *Fusion Eng. Des.*  
735 109 (2016) 1199–1206.
- 736 [93] M. Devillers, M. Sirch, S. Bredendiek-Kämper, R.D. Penzhorn, Characterization of the zirconium-cobalt  
737 (ZrCo)-hydrogen system in view of its use for tritium storage, *Chem. Mater.* 2 (1990) 255–262.
- 738 [94] T. Yamanishi, T. Hayashi, Y. Kawamura, Tritium accountancy and storage by hydrogen adsorption alloy  
739 in fusion fuel cycle, *Seramikkusu*. 46 (2011) 201–205.
- 740 [95] R.G. Budynas, J.K. Nisbett, Shigley’s mechanical engineering design, McGraw-Hill New York, 2008.
- 741 [96] V. Sears, Neutron scattering lengths and cross sections, *Neutron News*. (1992) 29–37.
- 742 [97] E.M. Schulson, D.B. Graham, The effect of transformation temperature on the hardness of the peritectoid  
743 phase Zr 3 Al, *J. Nucl. Mater.* 57 (1975) 358–360.
- 744 [98] E.M. Schulson, Zr3Al: a potential nuclear reactor structural material, *Intermet. Compd. Princ. Pract.*  
745 John Wiley Sons Ltd., Hoboken. (1994) 133–146.
- 746 [99] E.M. Schulson, J.A. Roy, The notch-sensitivity of ordered Zr3Al, *J. Nucl. Mater.* 71 (1977) 124–133.
- 747 [100] X.J. Jiang, Y.Y. Zhang, C.L. Li, G.D. Liang, R.H. Han, X.Y. Zhang, Microstructure and mechanical  
748 properties of ZrAl binary alloys, *J. Alloys Compd.* 811 (2019) 152068.
- 749 [101] E.M. Schulson, J.A. Roy, The yield strength of the L12 phase Zr3Al, *Acta Metall.* 26 (1978) 29–38.
- 750 [102] E.M. Schulson, The tensile and corrosion behaviour of ordered Zr3Al-based alloys, *J. Nucl. Mater.* 50  
751 (1974) 127–138.
- 752 [103] R. Kondo, N. Nomura, Y. Tsutsumi, H. Doi, T. Hanawa, Microstructure and mechanical properties of as-

- 753 cast Zr–Nb alloys, *Acta Biomater.* 7 (2011) 4278–4284.
- 754 [104] L. Chai, H. Wu, S. Wang, B. Luan, Y. Wu, X. Huang, Microstructural characteristics of cold-rolled Zr-  
755 2.5 Nb alloy annealed near the monotectoid temperature, *Sci. China Technol. Sci.* 61 (2018) 558–566.
- 756 [105] M. Griffiths, J.E. Winegar, A. Buyers, The transformation behaviour of the  $\beta$ -phase in Zr–2.5 Nb  
757 pressure tubes, *J. Nucl. Mater.* 383 (2008) 28–33.
- 758 [106] Z.N. Yang, X.B. Wang, F. Liu, F.C. Zhang, L.J. Chai, R.S. Qiu, L.Y. Chen, Effect of intercritical  
759 annealing temperature on microstructure and mechanical properties of duplex Zr-2.5 Nb alloy, *J. Alloys  
760 Compd.* 776 (2019) 242–249.
- 761 [107] B.S. Rodchenkov, A.N. Semenov, High temperature mechanical behavior of Zr–2.5% Nb alloy, *Nucl.  
762 Eng. Des.* 235 (2005) 2009–2018.
- 763 [108] G.J.C. Carpenter, E.F. Ibrahim, J.F. Watters, The aging response of zirconium-tin alloys, *J. Nucl. Mater.*  
764 102 (1981) 280–291.
- 765 [109] D. Arias, L. Roberti, The solubility of tin in  $\alpha$  and  $\beta$  zirconium below 1000 C, *J. Nucl. Mater.* 118 (1983)  
766 143–149.
- 767 [110] S.L. Wadekar, S. Banerjee, V. V Raman, M.K. Asundi, Correlation of microstructure and mechanical  
768 properties of Zr–Sn alloys, in: *Zircon. Nucl. Ind. Ninth Int. Symp.*, ASTM International, 1991.
- 769 [111] Z.H. Feng, C.Q. Xia, R. Jing, X.J. Jiang, Y.K. Zhou, H. Zhong, X.Y. Zhang, M.Z. Ma, R.P. Liu,  
770 Microstructure and mechanical properties of ZrBe alloys processed by hot rolling, *Mater. Sci. Eng. A.*  
771 667 (2016) 286–292.
- 772 [112] Z.H. Feng, C.Q. Xia, X.J. Jiang, S.G. Liu, X. Zhang, X.Y. Zhang, M.Z. Ma, R.P. Liu, Investigating the  
773 structure-property correlation of a novel Zirconium alloy by annealing treatment, *Mater. Sci. Eng. A.*  
774 677 (2016) 393–399.
- 775 [113] H.-C. Hsu, S.-C. Wu, S.-K. Hsu, Y.-C. Sung, W.-F. Ho, Effects of heat treatments on the structure and  
776 mechanical properties of Zr–30Ti alloys, *Mater. Charact.* 62 (2011) 157–163.
- 777 [114] S. Banerjee, R. Krishnan, Martensitic transformation in Zr– Ti alloys, *Metall. Trans.* 4 (1973) 1811–  
778 1819.
- 779 [115] H.-C. Hsu, S.-C. Wu, Y.-C. Sung, W.-F. Ho, The structure and mechanical properties of as-cast Zr–Ti  
780 alloys, *J. Alloys Compd.* 488 (2009) 279–283.
- 781 [116] Z.G. Zhang, Y.K. Zhou, X.J. Jiang, Z.H. Feng, C.Q. Xia, X.Y. Zhang, M.Z. Ma, R.P. Liu, A novel Zr-  
782 based alloy microstructure with high strength and excellent ductility, *Mater. Sci. Eng. A.* 651 (2016)  
783 370–375.
- 784 [117] Z.G. Zhang, Z.H. Feng, X.J. Jiang, X.Y. Zhang, M.Z. Ma, R.P. Liu, Microstructure and tensile properties  
785 of novel Zr–Cr binary alloys processed by hot rolling, *Mater. Sci. Eng. A.* 652 (2016) 77–83.
- 786 [118] C. Li, Y. Zhan, W. Jiang, Zr–Si biomaterials with high strength and low elastic modulus, *Mater. Des.* 32  
787 (2011) 4598–4602.
- 788 [119] M. Le Flem, J. Canel, S. Urvoy, Processing and characterization of Zr<sub>3</sub>Si<sub>2</sub> for nuclear applications, *J.*  
789 *Alloys Compd.* 465 (2008) 269–273.
- 790 [120] N. Nomura, K. Oya, Y. Tanaka, R. Kondo, H. Doi, Y. Tsutsumi, T. Hanawa, Microstructure and  
791 magnetic susceptibility of as-cast Zr–Mo alloys, *Acta Biomater.* 6 (2010) 1033–1038.
- 792 [121] A. V Nikulina, V.F. Konkov, M.M. Peregud, E.E. Vorobev, Effect of molybdenum on properties of  
793 zirconium components of nuclear reactor core, *Nucl. Mater. Energy.* 14 (2018) 8–13.
- 794 [122] H.C. Dong, Z.H. Feng, M.Z. Ma, X.Y. Zhang, R.P. Liu, Optimization of phase composition and  
795 mechanical properties in Zr alloys by micro-alloying, *Mater. Lett.* 202 (2017) 25–27.
- 796 [123] H. Ren, X. Liu, J. Ning, Microstructure and mechanical properties of W-Zr reactive materials, *Mater.*  
797 *Sci. Eng. A.* 660 (2016) 205–212.
- 798 [124] D. Araki, K. Kurosaki, H. Kimura, H. Muta, Y. Ohishi, K. Konashi, S. Yamanaka, Thermal and  
799 mechanical properties of hydrides of Zr–Hf alloys, *J. Nucl. Sci. Technol.* 52 (2015) 162–170.
- 800 [125] N.I. Taluts, A. V Dobromyslov, Structural and phase transformations in quenched and aged Zr–Os  
801 alloys, *J. Alloys Compd.* 298 (2000) 181–189.
- 802 [126] N.I. Taluts, A. V Dobromyslov, V.A. Elkin, Structural and phase transformations in quenched and aged  
803 Zr–Ru alloys, *J. Alloys Compd.* 282 (1999) 187–196.
- 804 [127] A. V Dobromyslov, N.I. Taluts, The formation of  $\alpha$  double-prime-phase in Zr–Re alloys, *Scr. Mater.* 35  
805 (1996) 573–577.
- 806 [128] J.-Q. Peng, Y. Chen, G.-Q. Yan, M. Wu, L.-J. Wang, J.-S. Li, Solid solubility extension and  
807 microstructure evolution of cast zirconium yttrium alloy, *Rare Met.* 35 (2016) 325–330.
- 808 [129] E. Fischer, C. Colinet, An updated thermodynamic modeling of the Al–Zr system, *J. Phase Equilibria  
809 Diffus.* 36 (2015) 404–413.
- 810 [130] I. Baker, E.M. Schulson, On grain boundaries in nickel-rich Ni<sub>3</sub>Al, *Scr. Metall.* 23 (1989) 1883–1886.
- 811 [131] H.E. Rosinger, The effect of neutron irradiation on the tensile properties and growth of zirconium-8.6  
812 wt% aluminum, Atomic Energy of Canada Ltd., 1976.

- 813 [132] E.M. Schulson, G.J.C. Carpenter, L.M. Howe, Irradiation swelling of Zr3Al, *J. Nucl. Mater.* 82 (1979)  
814 140–147.
- 815 [133] L.M. Howe, M.H. Rainville, A study of the irradiation behaviour of Zr3Al, *J. Nucl. Mater.* 68 (1977)  
816 215–234. [https://doi.org/https://doi.org/10.1016/0022-3115\(77\)90241-0](https://doi.org/https://doi.org/10.1016/0022-3115(77)90241-0).
- 817 [134] J.H. Li, Q. Li, F.C. Zhang, S. Liu, L. Mao, B.C. Hu, Z.N. Yang, Effects boron on microstructure and  
818 mechanical properties of Zr3Al-based alloys, *Mater. Lett.* 153 (2015) 70–72.
- 819 [135] E.M. Schulson, D.J. Cameron, Preparation of zirconium alloys, (1978).
- 820 [136] P. Fernández, A.M. Lancha, J. Lapeña, R. Lindau, M. Rieth, M. Schirra, Creep strength of reduced  
821 activation ferritic/martensitic steel Eurofer'97, *Fusion Eng. Des.* 75 (2005) 1003–1008.
- 822 [137] C.S. Seok, B. Marple, Y.J. Song, S. Gollapudi, I. Charit, K.L. Murty, High temperature deformation  
823 characteristics of Zirloy™ tubing via ring-creep and burst tests, *Nucl. Eng. Des.* 241 (2011) 599–602.
- 824 [138] R.S.W. Shewfelt, L.W. Lyall, D.P. Godin, A high-temperature creep model for Zr-2.5 wt% Nb pressure  
825 tubes, *J. Nucl. Mater.* 125 (1984) 228–235.
- 826 [139] B. Cox, Oxidation of zirconium-aluminum alloys, Atomic Energy of Canada Ltd., Chalk River, Ontario  
827 (Canada), 1967.
- 828 [140] E. V Murphy, R. Wieler, The corrosion behaviour of Zr 3 Al-based alloys, Atomic Energy of Canada  
829 Ltd., 1977.
- 830 [141] J. Ejenstam, Corrosion resistant alumina-forming alloys for lead-cooled reactors, (2015).
- 831 [142] M. Paljević, Z. Ban, Oxidation of stoichiometric Zr3Al-based alloy, *J. Nucl. Mater.* 95 (1980) 253–258.
- 832 [143] B.A. Cheadle, C.E. Coleman, H. Licht, CANDU-PHW pressure tubes: their manufacture, inspection, and  
833 properties, *Nucl. Technol.* 57 (1982) 413–425.
- 834 [144] S.B. Farina, A.G. Sanchez, S. Ceré, Effect of surface modification on the corrosion resistance of Zr-2.5  
835 Nb as material for permanent implants, *Procedia Mater. Sci.* 8 (2015) 1166–1173.
- 836 [145] B.S. Hickman, The formation of omega phase in titanium and zirconium alloys: a review, *J. Mater. Sci.*  
837 4 (1969) 554–563.
- 838 [146] T. Tokunaga, S. Matsumoto, H. Ohtani, M. Hasebe, Thermodynamic analysis of the phase equilibria in  
839 the Nb-Ni-Zr system, *Mater. Trans.* 48 (2007) 2263–2271.
- 840 [147] J.-P. Mardon, D. Charquet, J. Senevat, Influence of composition and fabrication process on out-of-pile  
841 and in-pile properties of M5 alloy, in: *Zircon. Nucl. Ind. Twelfth Int. Symp.*, ASTM International, 2000.
- 842 [148] A. Stern, J.-C. Brachet, V. Maillot, D. Hamon, F. Barcelo, S. Poissonnet, A. Pineau, J.-P. Mardon, A.  
843 Lesbros, Investigations of the microstructure and mechanical properties of prior-β structure as a function  
844 of the oxygen content in two zirconium alloys, *J. ASTM Int.* 5 (2008) 1–20.
- 845 [149] B. Cazalis, J. Desquines, C. Poussard, M. Petit, Y. Monerie, C. Bernaudat, P. Yvon, X. Averty, The  
846 PROMETRA program: Fuel cladding mechanical behavior under high strain rate, *Nucl. Technol.* 157  
847 (2007) 215–229.
- 848 [150] J. Wei, P. Frankel, E. Polatidis, M. Blat, A. Ambard, R.J. Comstock, L. Hallstadius, D. Hudson, G.D.W.  
849 Smith, C.R.M. Grovenor, The effect of Sn on autoclave corrosion performance and corrosion  
850 mechanisms in Zr–Sn–Nb alloys, *Acta Mater.* 61 (2013) 4200–4214.
- 851 [151] R.J. Pérez, C. Toffolon-Masclat, J.-M. Joubert, B. Sundman, The Zr–Sn binary system: New  
852 experimental results and thermodynamic assessment, *Calphad.* 32 (2008) 593–601.
- 853 [152] S.Y. Lee, K.T. Kim, S.I. Hong, Circumferential creep properties of stress-relieved Zircaloy-4 and Zr–  
854 Nb–Sn–Fe cladding tubes, *J. Nucl. Mater.* 392 (2009) 63–69.
- 855 [153] M.J. Rubel, V. Bailescu, J.P. Coad, T. Hirai, J. Likonen, J. Linke, C.P. Lungu, G.F. Matthews, L.  
856 Pedrick, V. Riccardo, Beryllium plasma-facing components for the ITER-Like Wall Project at JET, in: *J.*  
857 *Phys. Conf. Ser.*, IOP Publishing, 2008: p. 62028.
- 858 [154] Y. Mishima, N. Yoshida, H. Takahashi, K. Ishida, H. Kawamura, T. Iwadachi, T. Shibayama, I.  
859 Ohnuma, Y. Sato, K. Munakata, Present status of beryllides for fusion and industrial applications in  
860 Japan, *Fusion Eng. Des.* 82 (2007) 91–97.
- 861 [155] T. Tokunaga, H. Ohtani, M. Hasebe, Thermodynamic analysis of the Zr–Be system using  
862 thermochemical properties based on ab initio calculations, *Calphad.* 30 (2006) 201–208.
- 863 [156] L.E. Tanner, R. Ray, Metallic glass formation and properties in Zr and Ti alloyed with Be—I the binary  
864 Zr-Be and Ti-Be systems, *Acta Metall.* 27 (1979) 1727–1747.
- 865 [157] K.C.H. Kumar, P. Wollants, L. Delacy, Thermodynamic assessment of the Ti–Zr system and  
866 calculation of the Nb–Ti–Zr phase diagram, *J. Alloys Compd.* 206 (1994) 121–127.
- 867 [158] S.L. Sass, The structure and decomposition of Zr and Ti bcc solid solutions, *J. Less Common Met.* 28  
868 (1972) 157–173.
- 869 [159] W. Cui, Y. Liu, Fatigue behavior of Ti50Zr alloy for dental implant application, *J. Alloys Compd.* 793  
870 (2019) 212–219.
- 871 [160] Y.K. Zhou, S.X. Liang, R. Jing, X.J. Jiang, M.Z. Ma, C.L. Tan, R.P. Liu, Microstructure and tensile  
872 properties of hot-rolled Zr50–Ti50 binary alloy, *Mater. Sci. Eng. A.* 621 (2015) 259–264.

- 873 [161] H. Okamoto, Cr-Zr (chromium-zirconium), *J. Phase Equilibria*. 14 (1993) 768.
- 874 [162] C.T. Liu, J.H. Zhu, M.P. Brady, C.G. McKamey, L.M. Pike, Physical metallurgy and mechanical  
875 properties of transition-metal Laves phase alloys, *Intermetallics*. 8 (2000) 1119–1129.  
876 [https://doi.org/https://doi.org/10.1016/S0966-9795\(00\)00109-6](https://doi.org/https://doi.org/10.1016/S0966-9795(00)00109-6).
- 877 [163] M. Griffiths, A review of microstructure evolution in zirconium alloys during irradiation, *J. Nucl. Mater.*  
878 159 (1988) 190–218.
- 879 [164] J.J. Petrovic, A.K. Vasudevan, Key developments in high temperature structural silicides, *Mater. Sci.*  
880 *Eng. A*. 261 (1999) 1–5.
- 881 [165] H.M. Chen, Y. Xiang, S. Wang, F. Zheng, L.B. Liu, Z.P. Jin, Thermodynamic assessment of the C–Si–  
882 Zr system, *J. Alloys Compd.* 474 (2009) 76–80.
- 883 [166] C. Ramachandra, V. Singh, P.R. Rao, On silicides in high temperature titanium alloys, *Def. Sci. J.* 36  
884 (1986) 207–220.
- 885 [167] P. Barberis, N. Dupin, C. Lemaignan, A. Pasturel, J.M. Grange, Microstructure and phase control in Zr–  
886 Fe–Cr–Ni alloys: Thermodynamic and kinetic aspects, in: *Zircon. Nucl. Ind. Fourteenth Int. Symp.*,  
887 ASTM International, 2005.
- 888 [168] H. Zou, G.M. Hood, J.A. Roy, R.J. Schultz, Formation and stability of Fe-rich precipitates in dilute Zr  
889 (Fe) single-crystal alloys, *Metall. Mater. Trans. A*. 25 (1994) 1359–1365.
- 890 [169] C.-S. Zhang, B. Li, P.R. Norton, The segregation of Fe to a zirconium surface, *J. Nucl. Mater.* 223  
891 (1995) 238–244.
- 892 [170] Y. de Carlan, C. Regnard, M. Griffiths, D. Gilbon, C. Lemaignan, Influence of iron in the nucleation of(  
893 c) component dislocation loops in irradiated Zircaloy-4, in: *Zircon. Nucl. Ind. Elev. Int. Symp.*, ASTM  
894 International, 1996.
- 895 [171] Z. Karoutas, J. Brown, A. Atwood, L. Hallstadius, E. Lahoda, S. Ray, J. Bradfute, The maturing of  
896 nuclear fuel: Past to Accident Tolerant Fuel, *Prog. Nucl. Energy*. 102 (2018) 68–78.
- 897 [172] H. Okamoto, Mo-Zr (molybdenum-zirconium), *J. Phase Equilibria Diffus.* 25 (2004) 485.
- 898 [173] D.O. Northwood, Heat treatment, transformation reactions and mechanical properties of two high  
899 strength zirconium alloys, *J. Less Common Met.* 61 (1978) 199–212.
- 900 [174] C. Servant, Thermodynamic assessments of the phase diagrams of the hafnium-vanadium and vanadium-  
901 zirconium systems, *J. Phase Equilibria Diffus.* 26 (2005) 39–49.
- 902 [175] S.K. Lee, D.N. Lee, Calculation of phase diagrams using partial phase diagram data, *Calphad*. 10 (1986)  
903 61–76.
- 904 [176] N. Nomura, Y. Tanaka, R. Kondo, H. Doi, Y. Tsutsumi, T. Hanawa, Effects of phase constitution of Zr–  
905 Nb alloys on their magnetic susceptibilities, *Mater. Trans.* 50 (2009) 2466–2472.
- 906 [177] X.J. Jiang, Y.K. Zhou, Z.H. Feng, C.Q. Xia, C.L. Tan, S.X. Liang, X.Y. Zhang, M.Z. Ma, R.P. Liu,  
907 Influence of Zr content on  $\beta$ -phase stability in  $\alpha$ -type Ti–Al alloys, *Mater. Sci. Eng. A*. 639 (2015) 407–  
908 411.
- 909 [178] X.J. Jiang, R. Jing, C.Y. Liu, M.Z. Ma, R.P. Liu, Structure and mechanical properties of TiZr binary  
910 alloy after Al addition, *Mater. Sci. Eng. A*. 586 (2013) 301–305.
- 911 [179] X.J. Jiang, G. Yu, Z.H. Feng, C.Q. Xia, C.L. Tan, X.Y. Zhang, M.Z. Ma, R.P. Liu, Abnormal  $\beta$ -phase  
912 stability in TiZrAl alloys, *J. Alloys Compd.* 699 (2017) 256–261.
- 913 [180] C. Veiga, J.P. Davim, A.J.R. Loureiro, Properties and applications of titanium alloys: a brief review,  
914 *Rev. Adv. Mater. Sci.* 32 (2012) 133–148.
- 915 [181] R. Jing, S.X. Liang, C.Y. Liu, M.Z. Ma, X.Y. Zhang, R.P. Liu, Structure and mechanical properties of  
916 Ti–6Al–4V alloy after zirconium addition, *Mater. Sci. Eng. A*. 552 (2012) 295–300.
- 917 [182] S.X. Liang, M.Z. Ma, R. Jing, X.Y. Zhang, R.P. Liu, Microstructure and mechanical properties of hot-  
918 rolled ZrTiAlV alloys, *Mater. Sci. Eng. A*. 532 (2012) 1–5.
- 919 [183] Y.B. Tan, L.H. Yang, J.L. Duan, L.Y. Ji, W.C. Liu, Studies on the kinetics of  $\beta \rightarrow \alpha$  phase  
920 transformation in 47Zr–45Ti–5Al–3V alloy under isothermal conditions by X-ray diffraction, *Mater.*  
921 *Charact.* 112 (2016) 98–104.
- 922 [184] S.X. Liang, M.Z. Ma, R. Jing, C.L. Tan, R.P. Liu, Structural evolution and mechanical properties of Zr–  
923 45Ti–5Al–3V alloy by heat treatments, *Mater. Sci. Eng. A*. 541 (2012) 67–72.
- 924 [185] L. Qu, Z.N. Yang, F.C. Zhang, M. Zhang, X.Y. Zhang, R.P. Liu, Effect of deformation and heat  
925 treatment on the microstructure and mechanical properties of  $\beta$ -Zr40Ti5Al4V alloy, *J. Alloys Compd.*  
926 612 (2014) 80–89.
- 927 [186] J. Li, X. Zhang, J. Qin, M. Ma, R. Liu, Strength and grain refinement of Ti–30Zr–5Al–3V alloy by Fe  
928 addition, *Mater. Sci. Eng. A*. 691 (2017) 25–30.
- 929 [187] S.X. Liang, L.X. Yin, L.Y. Zheng, M.Z. Ma, R.P. Liu, Preparation of low cost TiZrAlFe alloy with ultra-  
930 high strength and favorable ductility, *Mater. Sci. Eng. A*. 639 (2015) 699–704.
- 931 [188] M.J.R. Barboza, C.M. Neto, C.R.M. Silva, Creep mechanisms and physical modeling for Ti–6Al–4V,  
932 *Mater. Sci. Eng. A*. 369 (2004) 201–209.

- 933 [189] L. Badea, M. Surand, J. Ruau, B. Viguier, Creep behavior of Ti-6Al-4V from 450° C to 600° C, (2014).
- 934 [190] G. Lütjering, J.C. Williams, A. Gysler, Microstructure and mechanical properties of titanium alloys, in:
- 935 Microstruct. Prop. Mater. (Volume 2), 2000: pp. 1–77.
- 936 [191] L. Nie, Y. Zhan, T. Hu, X. Chen, C. Wang, Novel high-strength ternary Zr–Al–Sn alloys with martensite
- 937 structure for nuclear applications, *J. Nucl. Mater.* 442 (2013) 100–105.
- 938 [192] L. Nie, Y. Zhan, H. Liu, C. Tang, Novel  $\beta$ -type Zr–Mo–Ti alloys for biological hard tissue replacements,
- 939 *Mater. Des.* 53 (2014) 8–12.
- 940 [193] L. Nie, Y. Zhan, T. Hu, X. Chen, C. Wang,  $\beta$ -Type Zr–Nb–Ti biomedical materials with high plasticity
- 941 and low modulus for hard tissue replacements, *J. Mech. Behav. Biomed. Mater.* 29 (2014) 1–6.
- 942 [194] P. Chui, Near  $\beta$ -type Zr–Nb–Ti biomedical alloys with high strength and low modulus, *Vacuum.* 143
- 943 (2017) 54–58.
- 944 [195] S.J. Zinkle, J.L. Boutard, D.T. Hoelzer, A. Kimura, R. Lindau, G.R. Odette, M. Rieth, L. Tan, H.
- 945 Tanigawa, Development of next generation tempered and ODS reduced activation ferritic/martensitic
- 946 steels for fusion energy applications, *Nucl. Fusion.* 57 (2017) 92005.
- 947 [196] D.J.M. King, S.C. Middleburgh, A.G. McGregor, M.B. Cortie, Predicting the formation and stability of
- 948 single phase high-entropy alloys, *Acta Mater.* 104 (2016) 172–179.
- 949 <https://doi.org/http://dx.doi.org/10.1016/j.actamat.2015.11.040>.
- 950 [197] J. Yeh, S. Chen, S. Lin, J. Gan, T. Chin, T. Shun, C. Tsau, S. Chang, Nanostructured High-Entropy
- 951 Alloys with Multiple Principal Elements: Novel Alloy Design Concepts and Outcomes, *Adv. Eng.*
- 952 *Mater.* (2004) 299–303.
- 953 [198] B. Cantor, I. Chang, P. Knight, A. Vincent, Microstructural development in equiatomic multicomponent
- 954 alloys, *Mater. Sci. Eng. A.* (2004) 213–218.
- 955 [199] D.B. Miracle, O.N. Senkov, A critical review of high entropy alloys and related concepts, *Acta Mater.*
- 956 122 (2017) 448–511.
- 957 [200] Y. Zhou, Y. Zhang, Y. Wang, G. Chen, Microstructure and compressive properties of multicomponent
- 958  $\text{Al}_x(\text{TiVCrMnFeCoNiCu})_{100-x}$  high-entropy alloys, *Mater. Sci. Eng. A.* (2007) 260–265.
- 959 [201] B.S. Li, Y.P. Wang, M.X. Ren, C. Yang, H.Z. Fu, Effects of Mn, Ti and V on the microstructure and
- 960 properties of AlCrFeCoNiCu high entropy alloy, *Mater. Sci. Eng. A.* 498 (2008) 482–486.
- 961 [202] Y.-L. Chen, Y.-H. Hu, C.-A. Hsieh, J.-W. Yeh, S.-K. Chen, Competition between elements during
- 962 mechanical alloying in an octonary multi-principal-element alloy system, *J. Alloys Compd.* 481 (2009)
- 963 768–775.
- 964 [203] Z. Wang, S. Guo, C.T. Liu, Phase Selection in High-Entropy Alloys: From Nonequilibrium to
- 965 Equilibrium, *JOM.* 66 (2014) 1966–1972. <https://doi.org/10.1007/s11837-014-0953-8>.
- 966 [204] S. Gorsse, M.H. Nguyen, O.N. Senkov, D.B. Miracle, Database on the mechanical properties of high
- 967 entropy alloys and complex concentrated alloys, *Data Br.* 21 (2018) 2664–2678.
- 968 [205] O.N. Senkov, D.B. Miracle, K.J. Chaput, J.-P. Couzinie, Development and exploration of refractory high
- 969 entropy alloys—A review, *J. Mater. Res.* (2018) 1–37.
- 970 [206] K. Jin, C. Lu, L.M. Wang, J. Qu, W.J. Weber, Y. Zhang, H. Bei, Effects of compositional complexity on
- 971 the ion-irradiation induced swelling and hardening in Ni-containing equiatomic alloys, *Scr. Mater.* 119
- 972 (2016) 65–70.
- 973 [207] O. El-Atwani, N. Li, M. Li, A. Devaraj, J.K.S. Baldwin, M.M. Schneider, D. Sobieraj, J.S. Wróbel, D.
- 974 Nguyen-Manh, S.A. Maloy, Outstanding radiation resistance of tungsten-based high-entropy alloys, *Sci.*
- 975 *Adv.* 5 (2019) eaav2002.
- 976 [208] D.J.M. King, S.T.Y. Cheung, S.A. Humphry-Baker, C. Parkin, A. Couet, M.B. Cortie, G.R. Lumpkin,
- 977 S.C. Middleburgh, A.J. Knowles, High temperature, low neutron cross-section high-entropy alloys in the
- 978 Nb–Ti–V–Zr system, *Acta Mater.* 166 (2019) 435–446.
- 979 <https://doi.org/https://doi.org/10.1016/j.actamat.2019.01.006>.

980  
981  
982  
983  
984  
985  
986  
987  
988  
989  
990

991  
992  
993  
994  
995  
996  
997  
998  
999  
1000  
1001  
1002  
1003  
1004  
1005  
1006  
1007  
1008  
1009  
1010  
1011  
1012  
1013  
1014  
1015  
1016  
1017  
1018  
1019  
1020  
1021  
1022

## Appendix

A simple spherical blanket model was created in OpenMC [1] using Constructive Solid Geometry (CSG) to ascertain the relative impact of different blanket material configurations on the tritium breeding ratio (TBR). The simplified model resembles inertial confinement fusion (ICF) reactors but avoids the introduction of design specific choices such as lack of inboard blankets and limits bias in the study. The aim is to provide relative TBR values as a stage in the process of down selecting from a wide range of materials, material fractions and dimensions. The radius of the vacuum region between neutron source and first wall is 10 m, the first wall armour and first wall thickness was based on Ref. [2] and set to 3 mm and 2.7 cm, respectively, and the blanket thickness was set at 2 m. A point source with a Muir energy distribution around 14.06 MeV was used to approximate a deuterium-tritium plasma neutron source, which is an available source term in OpenMC [4]. No backing was applied to the breeder zone to avoid biasing the result towards a design that depends on a reflection of neutrons. Nuclear data was used in from the following sources in the following order of preference Fendl 3.1d [6], Je\_ 3.3 [7] and ENDF 7.1 [8].

The neutronics material maker [5] was used to create individual materials as it takes account of variables such as temperature, pressure and  $^6\text{Li}$  enrichment when calculating material densities. The impacts the density of lithium lead and helium coolant is important to account for this when performing parameter scans. The amount of individual simulations required to accurately cover the parameter space is significant. To mitigate this, an adaptive sampling technique [9] was used to accurately cover the parameter range with a minimal number of simulations.

The material composition and volume fractions of the firstwall were fixed according to Table A1. The volume fractions of the structural and breeding material in the breeding zone were varied from 0 to 0.9. However, the volume fraction of the coolant in the breeder zone was fixed at 0.1, see Table A2. The breeder material was chosen as liquid Li-Pb ( $\text{Pb}_{84.2}\text{Li}_{15.8}$ ), due to the fact that ceramic breeders impose additional dimensions such as packing fraction and multiplier fraction. The  $^6\text{Li}$  enrichment was also been varied (from 0 - 100%) for this study. The specific structural materials that were investigated can be found in Table A3. The structural materials were homogenised together with a coolant and a breeder material to resemble a helium cooled lithium lead (HCLL) blanket design but is not a substitute for parameter studies performed on a specific heterogeneous design such as in Ref [3].

1023 Table A1: First wall composition, densities calculated using neutronics material maker [5]

Material	density (g/cm <sup>3</sup> )	volume fraction
Tungsten	19	0.106305
EUROFER 97	7.78	0.560188
Water at 15.5×10 <sup>6</sup> Pa and 305°C	0.72	0.333507
Helium at 8×10 <sup>6</sup> Pa and 500°C	0.0056	0.333507

1024

1025 Table A2: Breeder zone composition, densities calculated using neutronics material maker

1026 [5]

Material	density (g/cm <sup>3</sup> )		volume fraction
Variable structural material	variable		variable
Lithium-lead at 500°C	9.15		variable

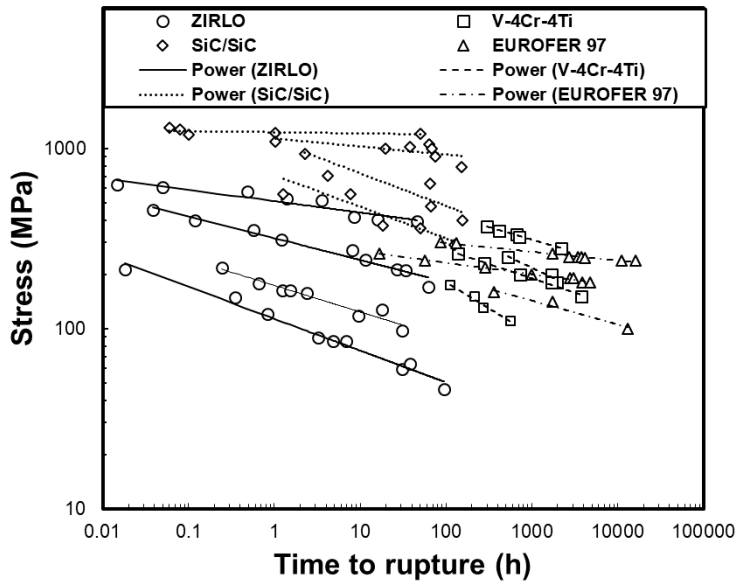
1027

1028 Table 3: Structural materials used in the simulation

Structural material	density (g/cm <sup>3</sup> )	elements and weight percents
EUROFER 97	7.8	Fe 89.27, C 0.11, Mn 0.4, Cr 9, Ta 0.12, W 1.1
Iron	7.87	Fe 100
SiC	2.7	Si 50, C 50
Vanadium	5.8	V 100
Vanadium 4	6.05	V 92, Cr 4, Ti, 4
Tungsten	19.3	W 100
Zircaloy 4	6.56	Zr 98.2, Sn 1.5, Fe 0.2, Cr 0.1
Zirconium	6.51	Zr 100
Zr <sub>3</sub> Al	5.91	Zr 75, Al 25

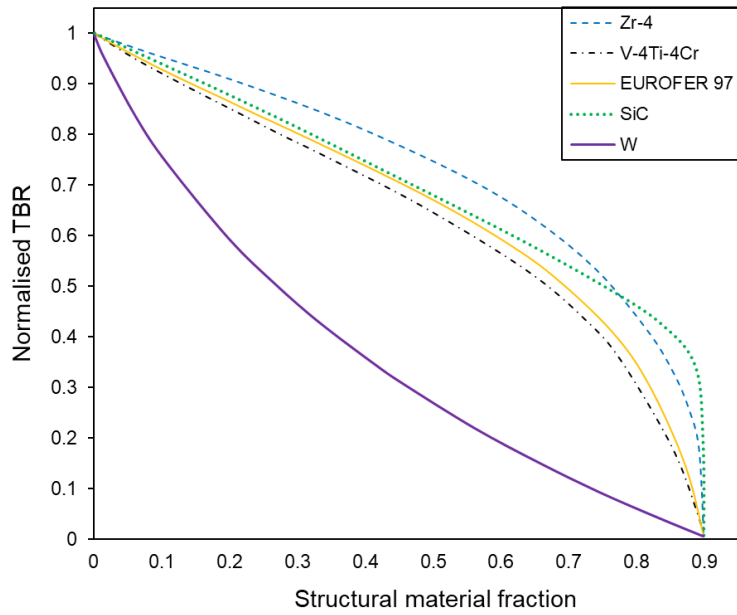
1029

1030



1031  
1032  
1033  
1034  
1035

Figure A1. Time to rupture of ZIRLO™ (circle), V-4Cr-4Ti (square), SiC/SiC (diamond) and EUROFER 97 (triangle) with



1036  
1037  
1038  
1039  
1040

Figure A2. The relative TBR with 0.9 <sup>6</sup>Li enrichment fraction for the WCLL design for different structural materials in the breeder blanket and the structural material fraction varied.